PVTOL Aerial Manipulators with a Rigid or an Elastic Joint: Analysis, Control, and Comparison

Burak Yüksel[1] and Antonio Franchi[2]

***Abstract*—In this paper we present the dynamic Lagrangian modeling, system analysis, and nonlinear control of a robot constituted by a planar-vtol (PVTOL) underactuated aerial vehicle equipped with a *rigid*- or an *elastic*-joint arm, which constitutes an *aerial manipulator*. For the design of the aerial manipulator, we first consider generic offsets between the center of mass (CoM) of the PVTOL, and the attachment point of the joint-arm. Later we consider a model in which these two points are the coinciding. It turns out to be that the choice of this attachment point is significantly affecting the capabilities of the platform. Furthermore, in both cases we consider the rigid- and elastic-joint arm configurations. For each of the resulting four cases we formally assess the presence of exact linearizing and differentially flat outputs and the possibility of using the dynamic feedback linearization (DFL) controller. Later we formalize an optimal control problem exploiting the differential flatness property of the systems, which is applied, as an illustrative example, to the *aerial throwing* task. Finally we provide extensive and realistic simulation results for comparisons between different robot models in different robotic tasks such as aerial grasping and aerial throwing, and a discussion on the applicability of computationally simpler controllers for the coinciding-point models to generic-point ones. Further exhaustive simulations on the trajectory tracking and the high-speed arm swinging capabilities are provided in a technical attachment.**

I. Introduction

Aerial robots are in use for scientific and technological development purposes that are increasing steadily over the last two decades. Thanks to the agility and the great workspace of such robots, they have been used to follow, e.g., complex trajectories [1], [2]. Such applications allowed researchers to develop new algorithms using mostly visual sensors for a vast range of fields [3], such as surveillance and patrolling, search and rescue, civil monitoring, agriculture and so on, and with or without the human in the loop [4].

Over the past few years, another application area of flying robots has been investigated deeply: *Aerial Physical Interaction* (APhI). In such applications, a flying robot is required to exert certain forces and/or torques (i.e., wrenches) to the environment, while maintaining a stable flight [5]. Examples of APhI are various; manipulation of an object [6], surface inspection [7], [8], object transportation [9], [10], or tool operation [11], just to mention a few. Moreover, various control methods for aerial manipulators have been developed, using, e.g., impedance control [12] or passive decomposition [13]. In [14] a mechanism moving the battery pack is included in the control framework for counterweighting the statics of the manipulator arm. Results of outdoor experiments are reported in [15], where authors have compared the performances of the PID and the backstepping controllers.

Although in most of the designs for aerial robots rigid actuators are considered, very recently some of the authors of this paper considered the use of a compliant (flexible) actuator together with a quadrotor aerial robot [16]. Mechanisms including compliant actuators, such as elastic-joint arms, have superiority over the rigid-joint arms when, e.g., the task requires the use of the energy stored in the elastic components to obtain faster dynamic ranges or a safer interaction with the environment. Examples for such tasks are, e.g., object throwing and hammering, which both require high velocities that a rigid-joint arm might not be able to provide, as well as safe human-robot physical interaction [17]. Such compliant mechanisms are widely used in *ground robots* like humanoids [18], in manipulators physically interacting with humans [17], and to achieve 'explosive' motion tasks [19]. Recently, a design of a light-weight compliant arm is presented in [20], where the authors showed the feasibility of the arm for payload mass estimation and collision detection. Despite the fact that the authors eventually plan to use this arm for aerial manipulation, the usage of such mechanisms in APhI and aerial manipulators is not yet fully investigated, with an only exception in [16], where design, identification and experiments of an elastic-joint arm on a quadrotor has been shown, with a controller driving the flying robot that however is unaware of the physical properties of the attached arm. In [16] it is experimentally shown that also in the aerial robot domain the use of an elastic-joint arm can amplify the link velocity compared to the rigid one, thanks to the energy stored in its elastic components. Moreover, the elastic joint provides passive compliance that is shown by the authors to be effective for aerial physical interaction tasks.

This paper is organized as follows. In Section II we present the motivation of this paper, and summarize our contributions to the literature. In Section III we first present the base model of the robot (PVTOL+joint+arm) considered in this paper and later formalize the objectives of our work. In Sec. IV-A, we recall the exact output tracking problem and in Section IV-B we systematically define the methods to achieve our objectives. In Section V-A the aerial manipulator model with a *Rigid*-joint arm attached on a *Generic* point is considered (Case RG), and the flat outputs of the system together with the dynamic state feedback linearization control law are provided. In Sec. V-B it is shown that for Case RG, the end-effector and PVTOL CoM positions of the aerial manipulator are not

[1]Max Planck Institute for Biological Cybernetics, Spemanstr. 38, 72076, Tübingen, Germany. burak.yueksel@tuebingen.mpg.de

[2]LAAS-CNRS, Université de Toulouse, CNRS, Toulouse, France, afranchi@laas.fr

part of the flat outputs. In Section V-C we show how the differential flatness property and the control design greatly improve when the Rigid-joint arm is attached to the *CoM* of the PVTOL (Case RC). In Section VI-A we show that a PVTOL with an *Elastic*-joint arm attached to a *Generic* point (Case EG), still possesses the differential flatness property and it is controllable though DFL, even though in a different and much more complex way. In Section VI-B we show that also in this case the flatness properties become much more powerful when the *Elastic*-joint arm is attached to the *CoM* of PVTOL (Case EC). In Section VII we show how to use differential flatness in the planning phase, and we formalize an optimal control problem for the considered aerial manipulator. In Section VIII we provide extensive and realistic simulation results and comparisons for various cases, such as trajectory tracking; control of the models of Cases RG and EG with the controllers of the Cases RC and EC, respectively (Sec. VIII-B); aerial grasping (Sec. VIII-C); high-speed arm swinging via link velocity amplification and object throwing using aerial manipulators (Sec. VIII-D). The results of the simulations are summarized in Section IX. Finally in Section X we conclude our work showing the bridge between the current work and our future plans.

II. Motivations and Paper Contributions

In this paper we consider an aerial manipulator with one DoF joint-arm. Such system can be considered as a more light-weight design compared to a redundant model. Although a redundant aerial manipulator can perform more dexterous tasks, the system we consider can easily achieve agile and explosive movement tasks as, e.g., aerial grasping or throwing. Notice that controlling such a system is not trivial, due to the underactuation, nonlinearity, and inertial coupling between the two systems.

Although the control of aerial robots [21] and the control of rigid or elastic joint type manipulators [22] have been studied in the literature separately, the analysis and control of systems consisting of these two, the so called *aerial manipulators*, is still an open (and rapidly growing) topic. In particular, the control of aerial manipulators with elastic arms has not been addressed so far and is not yet throughly understood. In this paper, we address the design and the control problems of this binomial, and propose four new nonlinear controllers for the four most important cases of aerial manipulator given by the possible combinations of the joint nature (rigid or elastic) with the kinematics of the platform-arm combination (generic attachment or CoM attachment), as summarized in Table I.

In this paper we aim at *i)* studying both the aerial vehicle and the manipulator together as one system, the *aerial manipulator, ii)* extending the preliminary insights shown in [16] and rigorously laying the foundations of the topic addressed there, and *iii)* comparing different designs of aerial manipulators for different tasks. We reach our goals by achieving the Objectives 1, 2 and 3 in Section III. To do so, we rigorously analyze the exact output tracking and differential flatness properties of different aerial manipulator designs, and propose dynamic feedback linearization control for each of them. A summary of the theoretical results can be found in Table II.

To the best of our knowledge, such an extensive study for aerial manipulators using differential flatness and exact linearizability has not been presented before. Furthermore, controlling the motion of a robot composed by an elastic-joint arm attached to a flying vehicle has not been studied yet. In this paper we fill this gap, by showing how we can independently and dynamically control the orientation of the elastic-joint arm together with the position of the PVTOL. By analyzing and proposing several controllers for robots of this novel type we aim at paving the way for the use of flexible-joint manipulators, which are able to benefit of the compliance advantages, also in the aerial physical interaction and manipulation field.

We exhaustively study the four different cases of Table I because each one is interesting for a different reason. First of all, the cases in which the joint is attached to any point of the PVTOL (shortly named 'Case RG' and 'Case EG' later) are interesting for their generality because they cover any possible real case. We prove that, in this case, the center of mass of the whole system (VTOL + arm) is a part flat of a output. On the other hand, we prove that the end-effector position is not in general part of a flat output, except for the cases in which the joint is attached to the CoM of the PVTOL, (shortly named 'Case RC' and 'Case EC' later). This fact brings strong advantages for the motion planning and control of the end-effector position because the whole state and the input can be computed analytically from a sufficiently smooth trajectory of the end-effector and the corresponding controllers are computationally simpler and do not generate a zero dynamics.

The rigid-joint cases (Case RG and Case RC) are found to be more suitable for tasks such as aerial grasping (see Sec. VIII-C) or trajectory tracking[1]. The reason is that elastic-joint need effort than rigid ones for these tasks, since the motors has to fight against the tendency of the spring to oscillate at its natural frequency. On the other hand the elastic-joint cases (Case EG and Case EC) are favorable for tasks in which one has to achieve high-speed link velocities such as aerial throwing (see Sec. VIII-D). The reason is the ability of the elastic components to store potential energy and release it in the form of kinetic energy.

Summarizing, the main contribution of this work is that we systematically provide *i)* a set of exact linearizing (i.e., flat) outputs for the all the four cases, *ii)* the explicit algebraic map from the flat outputs to the states and the control inputs, *iii)* a nonlinear controller for each case with formal proofs, *iv)* the formalization of an optimal control problem for aerial manipulators using differential flatness property, *v)* an extensive set of realistic numerical tests that shows its practicability with real robots, *vi)* a comparison between the rigid-joint and the elastic-joint cases that shows the benefits and drawbacks of each choice, *vii)* a numerical study on the robustness of the controller for the coinciding cases (Case RC and case EC)

[1]Additional simulation results are in the technical attachment. http://homepages.laas.fr/afranchi/files/J/TR-Yuesksel-Franchi.zip open with password: T-Ro2016.

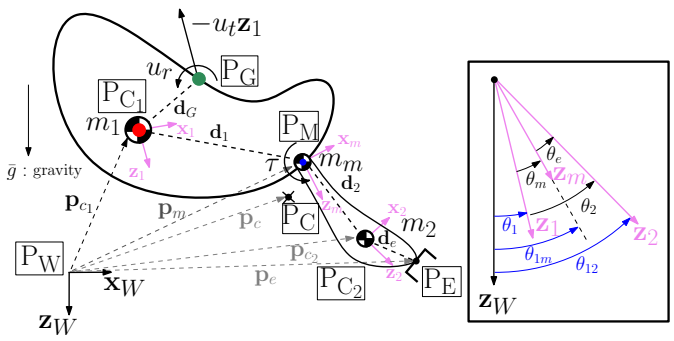


Fig. 1: – *Left:* a sketch of the mobile aerial manipulator, composed by a PVTOL equipped with a 1-link arm. Notice the offsets between: *i)* the center of mass (CoM) of the PVTOL ($\mathrm{P_{C_1}}$, red point), *ii)* the center of actuation of the PVTOL ($\mathrm{P_G}$, green point), and *iii)* the attachment point of the link ($\mathrm{P_M}$, blue point), around which the motor rotates and an either rigid or elastic joint is placed. – *Right:* relative and absolute angles of the rigid bodies. The lengths of the z axes are made different just for illustration purposes.

when the coinciding assumption is not exactly verified[2].

We note that a preliminary version of this paper was presented in [16], in which we only address the design and manufacturing problems. Here we present an extension of this work with a strong theoretical contribution.

III. Nomenclature and Objectives

In this section we provide the basic model of the robotic system and we formalize our objectives.

Similar to previous studies in robotics (see, e.g., [23]–[25]) we consider here the case of a planar vertical takeoff and landing (PVTOL) aerial platform. This kind of reduced system captures the main nonlinear features and the underactuation of a 3D system, and allows to generalize the obtained results in a later stage. Furthermore, many practical aerial problems are, fundamentally, 2D problems immersed in a 3D world (as, e.g., the aerial grasping problem addressed in [25]).

The considered mobile aerial manipulator is composed by a generic model of a PVTOL with an attached 1-link arm, as depicted in Fig. 1 (left). We denote with $\mathscr{F}_W : \{\mathrm{P_W}, \mathbf{x}_W, \mathbf{z}_W\}$ and $\mathscr{F}_1 : \{\mathrm{P_{C_1}}, \mathbf{x}_1, \mathbf{z}_1\}$, the world (inertial) frame and the frame attached to the PVTOL, respectively, where $\mathrm{P_{C_1}}$ is the Center of Mass (CoM) of the PVTOL (without the arm). Both the motor and the joint of the arm rotate about an axis parallel to $\mathbf{z}_W \times \mathbf{x}_W$ and passing through a point $\mathrm{P_M}$. We then define the *motor frame* as $\mathscr{F}_M : \{\mathrm{P_M}, \mathbf{x}_m, \mathbf{z}_m\}$ that is rigidly attached to the motor output shaft. The joint can be either rigid (cases considered in Sec. V) or elastic (cases considered in Sec. VI). We define also a *link frame* $\mathscr{F}_2 : \{\mathrm{P_{C_2}}, \mathbf{x}_2, \mathbf{z}_2\}$, where $\mathrm{P_{C_2}}$ is the CoM of the link. Finally we denote with the points $\mathrm{P_E}$ and $\mathrm{P_C}$ the end-effector of the arm and the CoM of the whole system (PVTOL+motor+link), respectively.

Given an angle $\theta_* \in \mathbb{R}$ between the z-axes of two frames, defined in Fig. 1 (right) we define:

$$\mathbf{R}_* = \begin{pmatrix} \cos\theta_* & \sin\theta_* \\ -\sin\theta_* & \cos\theta_* \end{pmatrix} \in \mathrm{SO}(2).$$

[2]Meaning that the attachment point of the arm and the PVTOL CoM are not coinciding, but the controllers are not aware of that.

	Rigid Joint	Elastic Joint
$\mathrm{P_{C_1}}$ and $\mathrm{P_M}$ are *generic*	Case **RG**, Sec.V-A	Case **EG**, Sec.VI-A
$\mathrm{P_{C_1}}$ and $\mathrm{P_M}$ are *coinciding*	Case **RC**, Sec.V-C	Case **EC**, Sec.VI-B

TABLE I: Summary of the aerial manipulator categories considered in this paper.

Therefore, the orientations of $\mathscr{F}_1$ in $\mathscr{F}_W$, $\mathscr{F}_M$ in $\mathscr{F}_1$, $\mathscr{F}_2$ in $\mathscr{F}_1$, and $\mathscr{F}_2$ in $\mathscr{F}_M$ are expressed by $\mathbf{R}_1$, $\mathbf{R}_m$, $\mathbf{R}_2$, and $\mathbf{R}_e$, respectively. The absolute motor angle is $\theta_{1m} = \theta_1 + \theta_m$ and absolute link angle is $\theta_{12} = \theta_1 + \theta_2$, as depicted with blue color in Fig. 1 (right). The angle $\theta_e = \theta_2 - \theta_m = \theta_{12} - \theta_{1m}$ is constantly zero if the joint is rigid and can be nonzero if the joint is elastic.

The constant positions of $\mathrm{P_M}$ and $\mathrm{P_G}$ in $\mathscr{F}_1$ are denoted with $\mathbf{d}_1 = [d_{1_x}\ d_{1_z}]^T \in \mathbb{R}^2$ and $\mathbf{d}_G = [d_{G_x}\ d_{G_z}]^T \in \mathbb{R}^2$ respectively. The constant position of $\mathrm{P_M}$ in $\mathscr{F}_2$ is denoted with $-\mathbf{d}_2 = [-d_{2_x}\ -d_{2_z}]^T \in \mathbb{R}^2$. Finally, the vector $\mathbf{d}_e = [d_{e_x}\ d_{e_z}]^T \in \mathbb{R}^2$ denotes the constant end-effector position $\mathrm{P_{C_2}}$ in $\mathscr{F}_2$.

The (time-varying) positions of $\mathrm{P_C}$, $\mathrm{P_{C_1}}$, $\mathrm{P_M}$, $\mathrm{P_{C_2}}$ and $\mathrm{P_E}$ in $\mathscr{F}_W$ are denoted with $\mathbf{p}_c = [x_c\ x_c]^T \in \mathbb{R}^2$, $\mathbf{p}_{c_1} = [x_1\ z_1]^T \in \mathbb{R}^2$, $\mathbf{p}_m = [x_m\ z_m]^T \in \mathbb{R}^2$, $\mathbf{p}_{c_2} = [x_2\ z_2]^T \in \mathbb{R}^2$, and $\mathbf{p}_e = [x_e\ z_e]^T \in \mathbb{R}^2$, respectively.

The mass and moment of inertia of the PVTOL, motor, and link are denoted with $m_1 \in \mathbb{R}_{>0}$, $J_1 \in \mathbb{R}_{>0}$; $m_m \in \mathbb{R}_{>0}$, $J_m \in \mathbb{R}_{>0}$; $m_2 \in \mathbb{R}_{>0}$, $J_2 \in \mathbb{R}_{>0}$, respectively. We use the symbol $\bar{g} \in \mathbb{R}^+$ to denote the gravitational constant.

The PVTOL is actuated by means of: *i)* a total *thrust force* $-u_t\mathbf{z}_1 \in \mathbb{R}^2$ applied at P_G, where u_t is its (signed) intensity and its direction $\mathbf{z}_1$ is constant in $\mathscr{F}_1$, and *ii)* a *total torque* (moment) $u_r(\mathbf{z}_1 \times \mathbf{x}_1) \in \mathbb{R}^2$ applied at P_G, where $u_r \in \mathbb{R}$ is its (signed) intensity.[3] Furthermore, a motor is attached to the PVTOL and applies a torque $\tau(\mathbf{z}_m \times \mathbf{x}_m) \in \mathbb{R}^2$ at $\mathrm{P_M}$ to the joint, where $\tau \in \mathbb{R}$ is its (signed) intensity. The three inputs of the system are gathered in the vector $\mathbf{u} = [u_t\ u_r\ \tau]^T \in \mathbb{R}^3$ and shortly denoted in the following as *thrust*, *PVTOL torque* and *motor torque*, respectively.

In this paper we shall consider the following cases: *i)* $\mathrm{P_{C_1}}$ and $\mathrm{P_M}$ are *generic*, i.e., there exist an arbitrary offset $\mathbf{d}_1 \in \mathbb{R}^2$ between each other; or *ii) coinciding*, i.e., $\mathbf{d}_1 = \mathbf{0}$. Moreover, for each of the previous cases we consider the case in which the connection between the PVTOL and 1-link arm is either *rigid* or *elastic*. Hence, four Cases are investigated in total, summarized in Table I.

Clearly, Case RC and Case EC are sub-cases of Case RG and Case EG, respectively. Nevertheless we shall show that they deserve a special treatment because new properties appear in those cases that significantly increase capabilities of the platform. Notice that in all cases the position of P_G can be any, i.e., $\mathbf{d}_G \in \mathbb{R}^2$ (while in the literature is typically assumed $P_G \equiv P_{C_1}$, i.e., $\mathbf{d}_G = \mathbf{0}$).

Like for similar mechanical systems, the robot dynamics can be expressed, using the Lagrange's equation, as

$$\ddot{\mathbf{q}} = \mathbf{M}^{-1}(\mathbf{q})\big(\mathbf{G}(\mathbf{q})\mathbf{u} - \mathbf{c}(\mathbf{q}, \dot{\mathbf{q}}) - \mathbf{g}(\mathbf{q}) + \mathbf{f}_E(\mathbf{q}) + \mathbf{f}_{ext}\big) \qquad (1)$$

[3]For example, in the case of a planar birotor, P_G would be the center of two coplanar propellers, u_t the sum of the forces provided by each propellers and u_r their difference times the distance from P_G, see, e.g., [26].

where $\mathbf{q} \in \mathbb{R}^n$ are the considered generalized coordinates ($n = 4$ for the rigid-joint cases whereas $n = 5$ for the elastic-joint cases), $\mathbf{M} \in \mathbb{R}^{n \times n}$ is the generalized mass and inertia matrix, $\mathbf{G} \in \mathbb{R}^{n \times 3}$ is the control input matrix, $\mathbf{c} \in \mathbb{R}^n$ stands for the centrifugal/Coriolis forces, $\mathbf{g} \in \mathbb{R}^n$ represents the gravitational forces, and $\mathbf{f}_E \in \mathbb{R}^n$ represents the forces due to the potential energy stored in the elastic joints (in the rigid-joint cases $\mathbf{f}_E = \mathbf{0}$). Finally, the external forces are denoted with $\mathbf{f}_{ext} \in \mathbf{R}^n$, and represent the force and torques applied to the system from the external environment. We shall specify the elements of (1) for each Case of Table I in the following sections.

Notice that in all the four cases the system is underactuated, because only three inputs are available for a system whose configuration space is either 4- or 5-dimensional.

For the PVTOL aerial manipulator considered in this paper we want to achieve the following objectives:

Objective 1. *(Trajectory generation) formally discover, if it exists, an exact linearizing (i.e., differentially flat) output and explicit the algebraic map from the flat output to the state* $\mathbf{q}, \dot{\mathbf{q}}$ *and the input* $\mathbf{u}$.

Objective 2. *(Control) Find the domain in which the decoupling matrix* $\bar{\mathbf{G}}$ *is invertible (see Sec. IV) and therefore a dynamic exact feedback linearization control is applicable.*

Objective 3. *(Rigid–Elastic Comparison) Compare the different cases, especially the elastic versus the rigid case in order to discover pros and cons of the two architectures.*

Note that it is a particularly challenging task to achieve the aforementioned Objectives for a PVTOL aerial manipulator due to the nonlinearity and underactuation of the system, and the presence of dynamical couplings between the floating base and the rigid- or elastic-joint arm.

IV. Control Background

For the reader convenience and the sake of completeness in this section we recall some concepts on exact output tracking. The experienced reader can quickly go over the section to retain only the symbol definitions.

A. Review of Exact Output Tracking

In order to state the goal of this work we briefly and rather informally recap some well known concepts in nonlinear control, see, e.g., [27] for a rigorous introduction to the topic. In the following we refer to a system in the form of (1).

Let be given an output $\mathbf{y}(\mathbf{q}) = [y_1\ y_2\ y_3]^T$ that is function of $\mathbf{q}$ and has the same size of $\mathbf{u}$ (i.e., three), and let us ask whether it is possible to make $\mathbf{y}$ track a desired trajectory $\mathbf{y}^d(t)$ whose derivatives are known and bounded, while maintaining the state $(\mathbf{q}, \dot{\mathbf{q}})$ and the input $\mathbf{u}$ bounded and with a known evolution that depends only on $\mathbf{y}^d(t)$ and its derivatives.

It is evident that finding an output possessing this strong property is very useful in practice. In fact, this is known as the *exact tracking control problem* and it is solvable if and only if $\mathbf{y}$ is an *exact linearizing output via dynamic feedback* for the system (1), which is defined in the following:

Definition 1. *An output* $\mathbf{y}$ *is an exactly linearizing output via dynamic feedback for* (1) *if it is possible to find* $s_1, s_2, s_3 \in \mathbf{N}_{\geq 0}$ *such that if one considers* $\bar{\mathbf{u}} = [u_1^{(s_1)}\ u_2^{(s_2)}\ u_3^{(s_3)}]^T$ *and* $\bar{\mathbf{x}} = [\mathbf{q}^T\ \dot{\mathbf{q}}^T\ u_1 \cdots u_1^{(s_1-1)}\ u_2 \cdots u_2^{(s_2-1)}\ u_3 \cdots u_3^{(s_3-1)}]^T$ *as the new input and the new state of the system, respectively,*[4] *then the the dynamics of* y_1, y_2, *and* y_3 *can be written as*

$$\bar{\mathbf{y}} = \begin{bmatrix} y_1^{(r_1)} & y_2^{(r_2)} & y_3^{(r_3)} \end{bmatrix}^T = \underbrace{\bar{\mathbf{f}}(\bar{\mathbf{x}})}_{\in \mathbb{R}^3} + \underbrace{\bar{\mathbf{G}}(\bar{\mathbf{x}})}_{\in \mathbb{R}^{3\times 3}} \bar{\mathbf{u}} \tag{2}$$

where the following conditions are verified

1) *the total relative degree* $r = r_1 + r_2 + r_3$ *matches with the dimension* $\bar{n}$ *of the augmented state, i.e.,*

$$r = r_1 + r_2 + r_3 = 2n + s_1 + s_2 + s_3 = \bar{n} \tag{3}$$

2) *the decoupling matrix* $\mathbf{G}(\bar{\mathbf{x}})$ *is invertible for some* $\bar{\mathbf{x}}$.

The name 'exactly linearizing' comes from the fact that if $\mathbf{y}$ is an exactly linearizing output, then input transformation

$$\bar{\mathbf{u}} = \bar{\mathbf{G}}^{-1}(\boldsymbol{\omega} - \bar{\mathbf{f}}) \tag{4}$$

brings the system in the linear controllable form

$$\bar{\mathbf{y}} = \boldsymbol{\omega} \tag{5}$$

which is equivalent to system (1) thanks to the matching condition on the relative degree (i.e., thanks to the absence of an internal dynamics).

Furthermore, the transformation (4) can also be used in a control scheme as inner linearizing control loop on top of which any linear pole placement or LQR control strategy can be employed [28] for the transformed system (5). However, the existence of an exact linearizing output is a general property of the system that is not necessarily related to the need of controlling it. In fact a system is said *exactly input-output linearizable via dynamic feedback* if it admits (at least) one exactly linearizing output, i.e., it exists a state and input change of coordinates (possibly including a state extension) which brings it to the simpler equivalent form (5).[5]

A similar concept introduced later in the literature (see, e.g., [29], [30]) is the one of *differentially flat system*.

Definition 2. *The system* (1) *is differentially flat if it exists an output* $\mathbf{y} = \begin{bmatrix} y_1 & y_2 & y_3 \end{bmatrix}^T$ *(called* flat output*) such that* $\mathbf{q}$, $\dot{\mathbf{q}}$, *and* $\mathbf{u}$ *can be expressed as an algebraic function of* y_1, y_2, y_3 *and a finite number of their derivatives.*

The presence of a flat output allows to know in advance (algebraically) the nominal state and input trajectories along which the system will evolve while tracking a desired output trajectory. Therefore it turns to be very useful in the planning and trajectory generation phase. Knowing that an output is flat allow also to use some flatness-based tracking control techniques, see, e.g., [31].

[4] Notice that $u_i^{(0)} = u_i$ and that $u_i^{(-1)}$ means that u_i does not belong to $\bar{\mathbf{x}}$.

[5] Note that here the obtained linear system is the same as the original one, i.e., the linearization is 'exact', and must not be confused with the linear approximation of a nonlinear system based on Taylor expansion and truncation at the first order.

The following important equivalence fact holds (see, e.g., [31], [32]):

Fact 1. *Differential flatness is equivalent to exact input-output linearizability via dynamic feedback in an open and dense set of the state space and an output is flat if and only if is exactly linearizing.*

B. Methodology

In this section, we describe the main steps of the method that we will shall employ in order to achieve the aforementioned Objectives 1 and 2.

Regarding Objective 1, in order to understand if an output is flat, one has to find an appropriate algebraic transformation. However, this is clearly not practical criteria, because it requires a priori knowledge if the output is flat or not, for a successful trial. On the other hand, Definition 1 provides a systematic way to assess whether an output is exactly linearizing or not. Moreover if it is, then one also finds a linearizing controller together with the differentially flat outputs, using Fact 1. Therefore, we will achieve Objective 1 using the following method:

Given an output $\mathbf{y}$:

1) we define the generalized coordinates $\mathbf{q}$ starting from $\mathbf{y}$ and adding one coordinate more in the rigid case and two more in the elastic case;
2) we compute $\mathbf{M}$, $\mathbf{c}$, $\mathbf{g}$, and $\mathbf{f}_E$ in (1) which makes possible to write down the exact dependency of each entry of $\ddot{\mathbf{y}}$ from each entry of $\mathbf{q}$, $\dot{\mathbf{q}}$, and $\mathbf{u}$, i.e.,
$$\ddot{y}_1 = f_1(\mathbf{q},\dot{\mathbf{q}},\mathbf{u})\ddot{y}_2 = f_2(\mathbf{q},\dot{\mathbf{q}},\mathbf{u}),\ \ddot{y}_3 = f_3(\mathbf{q},\dot{\mathbf{q}},\mathbf{u})\,; \quad (6)$$
3) using (6) and (1), we are able to compute the expected dependency of $y_i^{(j)}$ from each entry of $\mathbf{q}$, $\dot{\mathbf{q}}$, $\mathbf{u},\dot{\mathbf{u}},\ldots,\mathbf{u}^{(j-2)}$ for any $i = 1\ldots 3, j > 2$, without exactly computing the derivatives,
4) taking advantage of that we can easily compute, for each choice of s_1, s_2, s_3 what are the expected relative degrees r_1, r_2, and r_3 in (2), by just stopping as soon as one among $u^{(s_i)}$, $i = 1,\ldots,3$ appears for some j in $y_i^{(j)}$, thus having $r_i = j$
5) we can then check whether a choice exists for s_1, s_2, s_3 that possibly satisfies (3)
6) if this choice exists then we compute explicitly $\bar{\mathbf{G}}(\bar{\mathbf{x}})$ in (2) and we check for its invertibility in a certain domain of $\bar{\mathbf{x}}$ which implies that the output is exactly linearizing and, by virtue of Fact 1, also a flat output. by doing so we achieve Objective 2.

We refer the reader to Table II, for a summary of the result of this methodology applied to the four cases in exam. The proofs of the results will be given in the next sections.

Once we know that an output $\mathbf{y}$ is exactly linearizing we try to derive the algebraic relation described in Definition 2 which certainly exists, thus achieving Objective 1.

Objective 3 is achieved through the paper and mainly in Section VIII with realistic numerical tests.

V. PVTOL with a Rigid–Joint Arm

A. Rigid-joint Attached to a Generic Point (RG case)

In this section we consider the 'Case RG' in which P_{C_1} and P_M are generic, i.e., $\mathbf{d}_1 \in \mathbb{R}^2$, as shown with red and blue points in Fig. 1, respectively, and that the arm is attached through a rigid joint (top left case in Table I). Hence, the motor and the link orientation are the same, i.e., $\theta_m = \theta_2$. Notice that P_G (in green) can be anywhere, as in any other case considered in this paper.

In order to find an exactly linearizing (i.e., flat) output in this case let us choose some generalized coordinates which show no inertial couplings between translational and rotational part, i.e., $\mathbf{q} = [\mathbf{p}_c^T\ \theta_1\ \theta_{12}]^T \in \mathbb{R}^4$. With respect to these coordinates the generalized inertia matrix is found, after some algebra, as

$$\mathbf{M} = \begin{pmatrix} m_s\mathbf{I}_2 & * \\ \mathbf{0}_{2\times 2} & \mathbf{M}_r \end{pmatrix} = \mathbf{M}^T \in \mathbb{R}^{4\times 4}, \quad (7)$$

where $\mathbf{I}_i$ is $i \times i$ identity matrix, $\mathbf{0}_{i\times j}$ is a zero matrix in $\mathbb{R}^{i\times j}$,

$$\begin{aligned} \mathbf{M}_r &= \begin{pmatrix} m_a & * \\ m_{ab}(\theta_1,\theta_{12}) & m_b \end{pmatrix} \in \mathbb{R}^{2\times 2}, \\ m_a &= \frac{m_1(m_2+m_m)}{m_s}\|\mathbf{d}_1\|_2^2 + J_1, \\ m_b &= \frac{m_2(m_1+m_m)}{m_s}\|\mathbf{d}_2\|_2^2 + J_2 + J_m, \\ m_{ab}(\theta_1,\theta_{12}) &= \frac{m_1 m_2}{m_s}\mathbf{d}_1^T\mathbf{R}_2\mathbf{d}_2, \end{aligned} \quad (8)$$

with $\|\mathbf{d}_*\|_2^2 = \mathbf{d}_*^T\mathbf{d}_*$, $* = \{1,2\}$ and $m_s = m_1 + m_m + m_2$. The centrifugal/Coriolis and gravitational forces are

$$\mathbf{c}(\mathbf{q},\dot{\mathbf{q}}) = \begin{bmatrix} 0 \\ 0 \\ \frac{m_1 m_2}{m_s}\mathbf{d}_1^T\bar{\mathbf{R}}_2\mathbf{d}_2\dot{\theta}_{12}^2 \\ -\frac{m_1 m_2}{m_s}\mathbf{d}_1^T\bar{\mathbf{R}}_2\mathbf{d}_2\dot{\theta}_1^2 \end{bmatrix}, \quad \mathbf{g} = \begin{bmatrix} 0 \\ -m_s\bar{g} \\ 0 \\ 0 \end{bmatrix}, \quad (9)$$

where $\bar{\mathbf{R}}_* = \frac{\partial \mathbf{R}_*}{\partial \theta_*}$. The input matrix is

$$\mathbf{G}(\mathbf{q}) = \begin{pmatrix} -\sin\theta_1 & 0 & 0 \\ -\cos\theta_1 & 0 & 0 \\ -\frac{m_2+m_m}{m_s}d_{1_x} + d_{G_x} & 1 & -1 \\ -\frac{m_2}{m_s}(d_{2_x}\cos\theta_2 + d_{2_z}\sin\theta_2) & 0 & 1 \end{pmatrix}, \quad (10)$$

and, finally, thanks to the rigid connection, $\mathbf{f}_E = \mathbf{0}_{4\times 1}$.

Replacing $\mathbf{M}$, $\mathbf{c}$, $\mathbf{g}$, $\mathbf{G}$ and $\mathbf{f}_E$ in (1) we can derive the explicit dependency of each entry of $\ddot{\mathbf{q}}$, here summarized:

$$\begin{aligned} \ddot{x}_c &= f_1(\theta_1,u_t), \quad \ddot{z}_c = f_2(\theta_1,u_t) \\ \ddot{\theta}_1 &= f_3(\theta_1,\theta_{12},\dot{\theta}_1,\dot{\theta}_{12},u_t,u_r,\tau) \\ \ddot{\theta}_{12} &= f_4(\theta_1,\theta_{12},\dot{\theta}_1,\dot{\theta}_{12},u_t,u_r,\tau). \end{aligned} \quad (11)$$

We can observe from (11) that u_t is the only input appearing in $\ddot{x}_c$ and $\ddot{z}_c$. This implies that if we choose $s_1 > 0$ and include both x_c and z_c in the output, it is possible to let r increase twice as rapidly as $\bar{n}$ when we increase s_1, until an input other than u_t appears in the higher order derivatives of x_c or z_c (see Definition 1). Following this intuition, let us consider then $s_1 = 2$ and $s_2 = s_3 = 0$. We then obtain as new control inputs $\bar{\mathbf{u}} = [\ddot{u}_t\ u_r\ \tau]^T \in \mathbb{R}^3$, new state $\bar{\mathbf{x}} = [\mathbf{q}^T\ \dot{\mathbf{q}}^T\ u_t\ \dot{u}_t]^T \in \mathbb{R}^{10}$, and $\bar{n} = 10$.

Now, let us consider as output $\mathbf{y} = [\mathbf{p}_c^T \ \theta_{12}]^T = [\mathbf{y}_1^T \ y_2]^T$. Following the methodology presented in Section IV-B we then make clear the expected functional dependences without the need of explicitly computing the derivatives

$$\ddot{\mathbf{y}}_1 = \boldsymbol{f}_1(\theta_1, u_t), \quad \dddot{\mathbf{y}}_1 = \boldsymbol{f}_2(\theta_1, \dot{\theta}_1, u_t, \dot{u}_t)$$

and, substituting $\ddot{\theta}_1$ with f_3 in (11), we have

$$\ddddot{\mathbf{y}}_1 = \boldsymbol{f}_3(\theta_1, \theta_{12}, \dot{\theta}_1, \dot{\theta}_{12}, u_t, \dot{u}_t, \ddot{u}_t, u_r, \tau),$$

therefore $r_1 = r_2 = 4$. Considering also that, from (11), $r_3 = 2$, we have that $r_1 + r_2 + r_3 = 10 = \bar{n}$, which means that the Condition 1 of Definition 1 is satisfied. Therefore it is now worth investigating about the invertibility of $\bar{\mathbf{G}}(\bar{\mathbf{x}})$, which is done in the next proposition.

Proposition 1. *The vector $[\mathbf{p}_c^T \ \theta_{12}]^T$ is an exactly linearizing output via dynamic feedback for the generic model with rigid-joint arm (Case RG), as long as $u_t \neq 0$. As a consequence, it is also a flat output.*

Proof. Let us divide first the generalized coordinates into two parts; $\mathbf{q} = [\mathbf{p}_c^T \ \mathbf{q}_r^T]^T \in \mathbb{R}^4$, where $\mathbf{q}_r = [\theta_1 \ \theta_{12}]^T \in \mathbb{R}^2$. Then,

$$m_s \ddot{\mathbf{p}}_c = \mathbf{v} u_t + \begin{pmatrix} 0 \\ m_s \bar{g} \end{pmatrix}, \quad \mathbf{v} = \begin{pmatrix} -\sin\theta_1 \\ -\cos\theta_1 \end{pmatrix} \in \mathbb{R}^2. \tag{12}$$

Differentiating twice with respect to time we obtain

$$\begin{aligned} m_s \dddot{\mathbf{p}}_c &= \dot{\mathbf{v}} u_t + 2\dot{\mathbf{v}}\dot{u}_t + \mathbf{v}\ddot{u}_t, \quad \dot{\mathbf{v}} = \bar{\mathbf{v}}\dot{\theta}_1 \\ \ddot{\mathbf{v}} &= \bar{\mathbf{v}}\ddot{\theta}_1 - \mathbf{v}\dot{\theta}_1^2, \quad \bar{\mathbf{v}} = \frac{\partial \mathbf{v}}{\partial \theta_1} = \begin{pmatrix} -\cos\theta_1 \\ \sin\theta_1 \end{pmatrix} \end{aligned} \tag{13}$$

Now let us write the rotational dynamics of the system

$$\ddot{\mathbf{q}}_r = \begin{pmatrix} \ddot{\theta}_1 \\ \ddot{\theta}_{12} \end{pmatrix} = \mathbf{W} \begin{pmatrix} -c_3(\theta_1, \theta_{12}, \dot{\theta}_{12}) + g_{31} u_t + u_r + \tau \\ -c_4(\theta_1, \theta_{12}, \dot{\theta}_1) + g_{41}(\theta_1, \theta_{12}) u_t + \tau \end{pmatrix}, \tag{14}$$

where c_3 and c_4 are the 3-rd and 4-th elements of $\mathbf{c}$ in (9), and g_{31} and g_{41} are the 3-rd and 4-th elements of the first row of $\mathbf{G}$ in (10). Moreover, $\mathbf{W} = \mathbf{M}_r^{-1}$, where $\mathbf{M}_r$ is given in (8).

Now, use $\ddot{\theta}_1$ from the first column of (14) in (13) and $\ddot{\theta}_{12}$ from the last column of (14); and stack them together as

$$\begin{pmatrix} \dddot{\mathbf{p}}_c \\ \ddot{\theta}_{12} \end{pmatrix} = \mathbf{h}(\mathbf{q}_r, \dot{\mathbf{q}}_r, u_t, \dot{u}_t) + \bar{\mathbf{G}}\bar{\mathbf{u}}, \tag{15}$$

where

$$\underbrace{\left(\begin{array}{c|c|c} \frac{\mathbf{v}}{m_s} & \frac{\bar{\mathbf{v}}}{m_s} W_{11} u_t & \frac{\bar{\mathbf{v}}}{m_s}(W_{12} - W_{11}) u_t \\ \hline 0 & W_{12} & W_{22} - W_{11} \end{array}\right)}_{\bar{\mathbf{G}}} \underbrace{\begin{pmatrix} \ddot{u}_t \\ u_r \\ \tau \end{pmatrix}}_{\bar{\mathbf{u}}}. \tag{16}$$

The matrix $\bar{\mathbf{G}}$ is the new input matrix, with W_{ij} being the ij-th component of $\mathbf{W}$. After some algebra we can express the determinant of $\bar{\mathbf{G}}$ as

$$|\bar{\mathbf{G}}| = -\frac{u_t(W_{11}W_{22} - W_{12}^2)}{m_s^2} = -\frac{u_t |\mathbf{W}|}{m_s^2} = -\frac{u_t}{m_s^2 |\mathbf{M}_r|}, \tag{17}$$

meaning that $\bar{\mathbf{G}}$ is invertible as long as $u_t \neq 0$[6]. Furthermore it must hold $|\mathbf{M}_r| \neq 0$ for $\bar{\mathbf{G}}$ to be well-defined.

[6]Notice that all masses and inertias are positive.

Let us re-write the components of $\mathbf{M}_r$ in the following form

$$\begin{aligned} m_a &= m_\alpha \mathbf{d}_\alpha^T \mathbf{d}_\alpha + J_1 \\ m_b &= m_\beta \mathbf{d}_\beta^T \mathbf{d}_\beta + J_2 + J_m \\ m_{ab} &= m_\gamma \mathbf{d}_\alpha^T \mathbf{d}_\beta, \end{aligned} \tag{18}$$

with $\mathbf{d}_\alpha = \bar{\mathbf{R}}_1 \mathbf{d}_1$ and $\mathbf{d}_\beta = \bar{\mathbf{R}}_2 \mathbf{d}_2$, and $m_\alpha = \frac{m_1(m_2+m_m)}{m_s}$, $m_\beta = \frac{m_2(m_1+m_m)}{m_s}$ and $m_\gamma = \frac{m_1 m_2}{m_s}$. Then we can write

$$\begin{aligned} |\mathbf{M}_r| &= m_a m_b - m_{ab}^2 \\ &= m_{pos} + m_\alpha m_\beta (\mathbf{d}_\alpha^T \mathbf{d}_\alpha)(\mathbf{d}_\beta^T \mathbf{d}_\beta) - m_\gamma^2 (\mathbf{d}_\alpha^T \mathbf{d}_\beta)(\mathbf{d}_\alpha^T \mathbf{d}_\beta), \end{aligned} \tag{19}$$

where $m_{pos} = m_\alpha(J_2 + J_m)\mathbf{d}_\alpha^T \mathbf{d}_\alpha + m_\beta J_1 \mathbf{d}_\beta^T \mathbf{d}_\beta + J_1(J_2 + J_m) > 0$[7]. Notice that it is always $m_\alpha m_\beta > m_\gamma^2$. Moreover, $(\mathbf{d}_\alpha^T \mathbf{d}_\alpha)(\mathbf{d}_\beta^T \mathbf{d}_\beta) - (\mathbf{d}_\alpha^T \mathbf{d}_\beta)(\mathbf{d}_\alpha^T \mathbf{d}_\beta) = (d_{\alpha_1} d_{\beta_2} - d_{\alpha_2} d_{\beta_1})^2 > 0$ and it is always $(\mathbf{d}_\alpha^T \mathbf{d}_\alpha)(\mathbf{d}_\beta^T \mathbf{d}_\beta) > 0$, where d_{α_i} and $d_{\beta i}$ are the i-th components of $\mathbf{d}_\alpha$ and $\mathbf{d}_\beta$, respectively. Hence it is always $|\mathbf{M}_r| > 0$. This proofs that $[\mathbf{p}_c^T \ \theta_{12}]^T$ is exact linearizing output for Case RG. From Fact 1 it is differentially flat output as well. □

Derivation of the Algebraic Map from the Flat Output

We shall find now how to explicitly write down the algebraic map that relates $\ddot{\mathbf{p}}_c, \dddot{\mathbf{p}}_c, \ddddot{\mathbf{p}}_c, \theta_{12}, \dot{\theta}_{12}, \ddot{\theta}_{12}$ with θ_1, $\dot{\theta}_1$, and $\mathbf{u}$. Consider the first two equations of (11)

$$\begin{aligned} m_s \ddot{x}_c &= -\sin\theta_1 u_t \\ m_s \ddot{z}_c &= -\cos\theta_1 u_t + m_s \bar{g}. \end{aligned} \tag{20}$$

Define the vector $\mathbf{w} = \ddot{\mathbf{p}}_c - [0 \ \bar{g}]^T = [w_x \ w_z]^T \in \mathbb{R}^2$, which is a function of $\ddot{\mathbf{p}}_c$. It is clear that $\mathbf{w} = -\frac{u_t}{m_s}[\sin\theta_1 \ \cos\theta_1]^T$. Therefore $\theta_1 = \text{atan2}(w_z, w_x)$ and $u_t = m_s ||\mathbf{w}||$. Furthermore, differentiating $\theta_1(w_x, w_z)$ we obtain $\dot{\theta}_1(w_x, w_z, \dot{w}_x, \dot{w}_z)$ and $\ddot{\theta}_1(w_x, w_z, \dot{w}_x, \dot{w}_z, \ddot{w}_x, \ddot{w}_z)$, which are all functions of the derivatives of $\mathbf{p}_c$ from the second up to the fourth order. Then we can write

$$\begin{aligned} u_t &= m_s ||\mathbf{w}||, \quad \dot{u}_t = \frac{m_s w_1}{||\mathbf{w}||}, \quad \ddot{u}_t = -\frac{m_s \dot{w}_1}{||\mathbf{w}||} - \frac{m_s w_1^2}{||\mathbf{w}||^3}, \\ \dddot{u}_t &= \frac{m_s \ddot{w}_1}{||\mathbf{w}||} - \frac{3 m_s \dot{w}_1 w_1}{||\mathbf{w}||^3} + \frac{3 m_s w_1^2}{||\mathbf{w}||^5} \\ \ddddot{u}_t &= \frac{m_s \dddot{w}_1}{||\mathbf{w}||} - \frac{4 m_s w_1 \ddot{w}_1 + 3 m_s \dot{w}_1^2}{||\mathbf{w}||^3} + \\ &\quad + \frac{9 m_s \dot{w}_1 w_1^2 + 6 m_s w_1 \dot{w}_1}{||\mathbf{w}||^5} - \frac{15 m_s w_1^3}{||\mathbf{w}||^7}, \end{aligned} \tag{21}$$

where

$$\begin{aligned} ||\mathbf{w}|| &= \sqrt{\ddot{p}_{c_x}^2 + \ddot{p}_{c_z}^2 - 2\ddot{p}_{c_z}\bar{g} + \bar{g}^2} \\ w_1 &= \dddot{p}_{c_x} \ddot{p}_{c_x} + \dddot{p}_{c_z} (\ddot{p}_{c_z} - \bar{g}) \\ \dot{w}_1 &= \ddddot{p}_{c_x} \ddot{p}_{c_x} + \dddot{p}_{c_x}^2 + \dddot{p}_{c_z}^2 + \ddddot{p}_{c_z} (\ddot{p}_{c_z} - \bar{g}) \\ \ddot{w}_1 &= p_{c_x}^{(5)} \ddot{p}_{c_x} + 3\ddddot{p}_{c_x} \dddot{p}_{c_x} + 3\ddddot{p}_{c_z} \dddot{p}_{c_z} + p_{c_z}^{(5)} (\ddot{p}_{c_z} - \bar{g}) \\ \dddot{w}_1 &= p_{c_x}^{(6)} \ddot{p}_{c_x} + 4 p_{c_x}^{(5)} \dddot{p}_{c_x} + 3\ddddot{p}_{c_x}^2 + 3\ddddot{p}_{c_z}^2 + 4 p_{c_z}^{(5)} \dddot{p}_{c_z} + p_{c_z}^{(6)} (\ddot{p}_{c_z} - \bar{g}), \end{aligned}$$

[7]Recall that $\mathbf{d}_\alpha^T \mathbf{d}_\alpha = ||\mathbf{d}_1||_2^2 > 0$ and $\mathbf{d}_\beta^T \mathbf{d}_\beta = ||\mathbf{d}_2||_2^2 > 0$, as also stated in (8).

where $\dddot{u}_t$ and $\ddddot{u}_t$ are provided for the convenience of the further analyses. Moreover we can write[8]

$$\begin{aligned}\theta_1 &= \text{atan2}(w_z, w_x), \quad w_z = \ddot{p}_{c_z} - \bar{g},\ w_x = \ddot{p}_{c_x}\\ \dot{\theta}_1 &= \frac{\dot{w}_x w_z - w_x \dot{w}_z}{w_x^2 + w_z^2} = \frac{\dddot{p}_{c_x}(\ddot{p}_{c_z} - \bar{g}) - \ddot{p}_{c_x}\dddot{p}_{c_z}}{\ddot{p}_{c_x}^2 + (\ddot{p}_{c_z} - \bar{g})^2}\\ \ddot{\theta}_1 &= \frac{\ddot{w}_x w_z - w_x \ddot{w}_z}{(w_x^2 + w_z^2)} - \frac{2\left[(w_z^2 - w_x^2)\dot{w}_x \dot{w}_z + (\dot{w}_x^2 - \dot{w}_z^2) w_x w_z\right]}{(w_x^2 + w_z^2)^2},\end{aligned} \tag{22}$$

where

$$\dot{w}_x = \dddot{p}_{c_x}, \quad \ddot{w}_x = \ddddot{p}_{c_x}, \quad \dot{w}_z = \dddot{p}_{c_z}, \quad \ddot{w}_z = \ddddot{p}_{c_z}.$$

Now considering the last equation of the system dynamics, we can retrieve the motor torque as

$$\begin{aligned}\tau = \tau(\theta_{12}, \ddot{\theta}_{12}, \theta_1, \dot{\theta}_1, \ddot{\theta}_1, u_t) = m_{ab}(\theta_1, \theta_{12})\ddot{\theta}_1 + m_b \ddot{\theta}_{12} -\\ - \frac{m_1 m_2}{m_s}\mathbf{d}_1^T \bar{\mathbf{R}}_2(\theta_1, \theta_{12})\mathbf{d}_2 \dot{\theta}_1^2 + \left(\frac{m_2 + m_m}{m_s} d_{1_x} - d_{G_x}\right) u_t\end{aligned}$$

and using θ_1, $\dot{\theta}_1$, $\ddot{\theta}_1$ from (22) and u_t from (21), we show that $\tau = \tau(\ddot{\mathbf{y}}_1, \dddot{\mathbf{y}}_1, \ddddot{\mathbf{y}}_1, y_2, \dot{y}_2)$. Now, replacing τ from above into the third equation of the system dynamics we have

$$\begin{aligned}u_r = u_r(\theta_{12}, \dot{\theta}_{12}, \ddot{\theta}_{12}, \theta_1, \dot{\theta}_1, \ddot{\theta}_1, u_t) = m_a \ddot{\theta}_1 + m_b \ddot{\theta}_{12} +\\ + m_{ab}(\theta_1, \theta_{12})(\ddot{\theta}_1 + \ddot{\theta}_{12}) + \frac{m_1 m_2}{m_s}\mathbf{d}_1^T \bar{\mathbf{R}}_2(\theta_1, \theta_{12})\mathbf{d}_2(\dot{\theta}_{12}^2 - \dot{\theta}_1^2) +\\ + \Big(\frac{m_2 + m_m}{m_s} d_{1_x} - d_{G_x} + \frac{m_2}{m_s}(d_{2_x}\cos\theta_2 + d_{2_z}\sin\theta_2)\Big) u_t,\end{aligned}$$

where by substituting θ_1, $\dot{\theta}_1$, $\ddot{\theta}_1$ from (22) and u_t from (21), we have $u_r = u_r(\ddot{\mathbf{y}}_1, \dddot{\mathbf{y}}_1, \ddddot{\mathbf{y}}_1, y_2, \dot{y}_2, \ddot{y}_2)$.

In summary, we obtained $\mathbf{p}_c = \mathbf{y}_1$, $\dot{\mathbf{p}}_c = \dot{\mathbf{y}}_1$, $\ddot{\mathbf{p}}_c = \ddot{\mathbf{y}}_1$ and $\theta_{12} = y_2$, $\dot{\theta}_{12} = \dot{y}_2$, $\ddot{\theta}_{12} = \ddot{y}_2$ from the definition; $u_t = u_t(\ddot{\mathbf{y}}_1)$, $\dot{u}_t = \dot{u}_t(\ddot{\mathbf{y}}_1, \dddot{\mathbf{y}}_1)$, $\ddot{u}_t = \ddot{u}_t(\ddot{\mathbf{y}}_1, \dddot{\mathbf{y}}_1, \ddddot{\mathbf{y}}_1)$ from (21); $\theta_1 = \theta_1(\ddot{\mathbf{y}}_1)$, $\dot{\theta}_1 = \dot{\theta}_1(\ddot{\mathbf{y}}_1, \dddot{\mathbf{y}}_1)$, $\ddot{\theta}_1 = \ddot{\theta}_1(\ddot{\mathbf{y}}_1, \dddot{\mathbf{y}}_1, \ddddot{\mathbf{y}}_1)$ from (22); and finally $\tau = \tau(\ddot{\mathbf{y}}_1, \dddot{\mathbf{y}}_1, \ddddot{\mathbf{y}}_1, y_2, \ddot{y}_2)$ and $u_r = u_r(\ddot{\mathbf{y}}_1, \dddot{\mathbf{y}}_1, \ddddot{\mathbf{y}}_1, y_2, \dot{y}_2, \ddot{y}_2)$ as shown above[9]. Hence we showed the states and the control inputs of the system as functions of the flat outputs and their finite number of derivatives.

Remark 1. *Although dependencies of* $\ddot{\theta}_1$ *and* $\ddot{\theta}_{12}$ *in* (11) *are the same,* $\mathbf{y} = [\mathbf{p}_c^T\ \theta_1]^T$ *is not an exactly linearizing output, because in this case it is possible to show that* $\det(\bar{\mathbf{G}}) = 0$.

B. Impossibility of Exact Tracking of the End-effector Position

In the most interesting cases for aerial manipulation, one needs to control the end-effector position $\mathbf{p}_e$ instead of $\mathbf{p}_c$. In this section we introduce a negative result that shows how unfortunately this objective is not feasible for the Case RG.

The expression of $\mathbf{p}_e$ in function of $\mathbf{q}$ is:

$$\begin{aligned}\mathbf{p}_e &= f(\mathbf{p}_c, \theta_1, \theta_{12})\\ &= \mathbf{p}_c + \frac{m_1}{m_s}\mathbf{R}_1 \mathbf{d}_1 + \mathbf{R}_{12}\Big(\frac{m_1 + m_m}{m_s}\mathbf{d}_2 + \mathbf{d}_e\Big)\end{aligned} \tag{23}$$

which shows that $\mathbf{p}_e$ cannot be computed using only the flat output $[\mathbf{p}_c^T\ \theta_{12}]^T$ since also θ_1 is required in (23). Therefore it is impossible to let exactly $\mathbf{p}_e$ track a desired trajectory $\mathbf{p}_e^d(t)$ using control methods based on the flat output $[\mathbf{p}_c^T\ \theta_{12}]^T$.

On the other hand, since

$$\mathbf{p}_e = \mathbf{p}_m + \mathbf{R}_{12}(\mathbf{d}_2 + \mathbf{d}_e) \tag{24}$$

one can let $\mathbf{p}_e$ exactly track $\mathbf{p}_e^d$, if $[\mathbf{p}_m^T\ \theta_{12}]^T \in \mathbb{R}^3$ is a flat output as well. In order to discover if and under which conditions $[\mathbf{p}_m^T\ \theta_{12}]^T \in \mathbb{R}^3$ is a flat output, let us write the dynamics of the system for the generalized coordinates $\mathbf{q} = [\mathbf{p}_m^T\ \theta_1\ \theta_{12}]^T$. With respect to these coordinates, the generalized inertia matrix becomes

$$\mathbf{M} = \begin{pmatrix} m_s \mathbf{I}_2 & * & * \\ \boldsymbol{\alpha}^T(\theta_1) & m_A & * \\ \boldsymbol{\beta}^T(\theta_{12}) & 0 & m_B \end{pmatrix} = \mathbf{M}^T \in \mathbb{R}^{4\times 4}, \tag{25}$$

where

$$\begin{aligned} m_A &= m_1 \|\mathbf{d}_1\|_2^2 + J_1 & m_B &= m_2 \|\mathbf{d}_2\|_2^2 + J_2 + J_m\\ \boldsymbol{\alpha}(\theta_1) &= -m_1 \bar{\mathbf{R}}_1 \mathbf{d}_1 \in \mathbb{R}^2 & \boldsymbol{\beta}(\theta_{12}) &= m_2 \bar{\mathbf{R}}_{12}\mathbf{d}_2 \in \mathbb{R}^2. \end{aligned} \tag{26}$$

The centrifugal/Coriolis and gravitational forces are

$$\mathbf{c}(\mathbf{q}, \dot{\mathbf{q}}) = \begin{bmatrix} \bar{\alpha}_1(\theta_1)\dot{\theta}_1^2 + \bar{\beta}_1(\theta_{12})\dot{\theta}_{12}^2 \\ \bar{\alpha}_2(\theta_1)\dot{\theta}_1^2 + \bar{\beta}_2(\theta_{12})\dot{\theta}_{12}^2 \\ 0 \\ 0 \end{bmatrix}, \quad \mathbf{g}(\mathbf{q}) = \begin{bmatrix} 0 \\ -m_s \bar{g} \\ g_3(\theta_1) \\ g_4(\theta_{12}) \end{bmatrix}, \tag{27}$$

with $\bar{\boldsymbol{\beta}} = \frac{\partial \boldsymbol{\beta}}{\partial \theta_{12}} = [\bar{\beta}_1\ \bar{\beta}_2]^T \in \mathbb{R}^2$, and

$$\begin{aligned} \bar{\alpha}_1 &= m_1(d_{1_x}\cos(\theta_1) + d_{1_z}\sin(\theta_1))\\ \bar{\alpha}_2 &= m_1(d_{1_z}\cos(\theta_1) - d_{1_x}\sin(\theta_1))\\ \bar{\beta}_1 &= -m_2(d_{2_x}\cos(\theta_{12}) + d_{2_z}\sin(\theta_{12}))\\ \bar{\beta}_2 &= -m_2(d_{2_z}\cos(\theta_{12}) - d_{2_x}\sin(\theta_{12}))\\ g_3 &= -m_1 \bar{g}(d_{1_x}\cos(\theta_1) + d_{1_z}\sin(\theta_1))\\ g_4 &= m_2 \bar{g}(d_{2_x}\cos(\theta_{12}) + d_{2_z}\sin(\theta_{12})). \end{aligned} \tag{28}$$

The input matrix is

$$\mathbf{G}(\mathbf{q}) = \begin{pmatrix} -\sin\theta_1 & 0 & 0 \\ -\cos\theta_1 & 0 & 0 \\ -d_{1_x} + d_{G_x} & 1 & -1 \\ 0 & 0 & 1 \end{pmatrix}, \tag{29}$$

and, as in the previous case, $\mathbf{f}_E = \mathbf{0}_{4\times 1}$.

Let us now ask ourselves if $\mathbf{y} = [\mathbf{p}_m^T\ \theta_{12}]^T$ is an exactly linearizing output via dynamic feedback (i.e., a flat output). Due to the inertial coupling, $\ddot{\mathbf{y}}$ depends from all the control inputs, therefore the gap between $\bar{n} - r = 2$ will stay for any choice of s_1, s_2, and s_3, which shows that $\ddot{\mathbf{y}}$ is not exactly linearizing and therefore is not flat.

Corollary 1. *The vectors* $[\mathbf{p}_m^T\ \theta_{12}]^T$, $[\mathbf{p}_{c_1}^T\ \theta_{12}]^T$ *and* $[\mathbf{p}_e^T\ \theta_{12}]^T$ *are* not *an exactly linearizing output via dynamic feedback for the generic model with rigid-joint arm (Case RG). As a consequence, they are* not *flat outputs either.*

C. Rigid-joint Attached to the PVTOL CoM (RC case)

The negative result of Corollary 1 is a consequence of the strong inertial coupling in (25). In this section we show that if we consider a model in which $\mathrm{P}_{\mathrm{C}_1}$ coincides with P_{M}, i.e., $\mathbf{p}_{c_1} = \mathbf{p}_m$, then the inertial coupling weakens enough to make $[\mathbf{p}_m^T\ \theta_{12}]^T$ an exactly linearizing (i.e., flat) output for the system

[8] in the range of θ_1, in which the derivatives of $\text{atan2}(w_z, w_x)$ exist.

[9] Notice that the high order derivatives of the flat outputs can be computed analytically using (1).

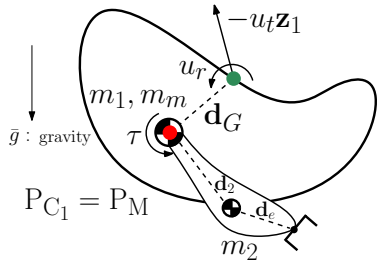


Fig. 2: A sketch of the PVTOL aerial manipulator for the cases in which the attachment point of the rigid-joint arm is same with the CoM of the PVTOL ($\mathrm{P}_{\mathrm{C}_1} = \mathrm{P}_{\mathrm{M}}$), i.e., Case RC and Case EC. Notice that the point of application of the thrust is still any (i.e., $\mathbf{d}_G \in \mathbb{R}^2$).

in exam[10]. In order to prove that, let us choose as generalized coordinates $\mathbf{q} = [\mathbf{p}_m^T \ \theta_1 \ \theta_{12}]^T \in \mathbb{R}^4$. The dynamic model for these coordinates are given in Section V-B. Now assume that $\mathbf{p}_{c_1} = \mathbf{p}_m$. Such case is depicted in Fig. 2, where motor and the joint are placed at the CoM of the PVTOL. This is a special case of the generic model, that we call the *coinciding model with rigid joint*[11] (Case RC in Table I).

Consider the dynamic model given in Section V-B with $\mathbf{d}_1 = \mathbf{0}_{2\times 1}$ (because of the coinciding assumption). We obtain the following simplifications in some of previous expressions:

$$m_A = J_1 \tag{30}$$
$$\boldsymbol{\alpha}(\theta_1) = \mathbf{0}_{2\times 1} \tag{31}$$
$$\bar{\alpha}_1(\theta_1) = \bar{\alpha}_2(\theta_1) = g_3(\theta_1) = 0. \tag{32}$$

Moreover, $d_{1_x} = 0$ in (29).

The explicit functional dependency of $\ddot{\mathbf{q}}$ then becomes[12]

$$\begin{aligned} &\ddot{x}_m = f_1(\theta_1, \theta_{12}, \dot{\theta}_{12}, u_t, \tau), \quad \ddot{z}_m = f_2(\theta_1, \theta_{12}, \dot{\theta}_{12}, u_t, \tau) \\ &\ddot{\theta}_1 = f_3(u_t, u_r, \tau), \quad \ddot{\theta}_{12} = f_4(\theta_1, \theta_{12}, \dot{\theta}_{12}, u_t, \tau), \end{aligned} \tag{33}$$

where we see that now u_r does not appear anymore in neither $\ddot{\mathbf{p}}_m$ nor $\ddot{\theta}_{12}$, as it was instead happening in Case RG. Therefore if we choose $\mathbf{y} = [\mathbf{p}_m^T \ \theta_{12}]^T$ as the output, we obtain from (33)

$$\ddot{\mathbf{y}} = \boldsymbol{f}_1(\theta_1, \theta_{12}, \dot{\theta}_{12}, u_t, \tau). \tag{34}$$

The fact that the two inputs u_t and τ are the only appearing in the three input channels implies that if we choose both $s_1 > 0$ and $s_3 > 0$, it is possible to let r increase more rapidly than $\bar{n}$ when we increase s_1 and s_3, until the input u_r appears in the higher order derivatives of $\mathbf{y}$ (see Definition 1). Following this intuition, let us consider then $s_1 = 2$, $s_3 = 2$ and $s_2 = 0$. We then obtain as new control inputs $\bar{\mathbf{u}} = [\ddot{u}_t \ u_r \ \ddot{\tau}]^T \in \mathbb{R}^3$, new state $\bar{\mathbf{x}} = [\mathbf{q}^T \ \dot{\mathbf{q}}^T \ u_t \ \dot{u}_t \ \tau \ \dot{\tau}]^T \in \mathbb{R}^{12}$, and $\bar{n} = 12$.

Considering that $\ddot{\theta}_{12}$ is available from f_4 of (33) we write

$$\dddot{\mathbf{y}} = \boldsymbol{f}_2(\theta_1, \theta_{12}, \dot{\theta}_1, \dot{\theta}_{12}, u_t, \tau, \dot{u}_t, \dot{\tau}) \tag{35}$$

and, substituting $\ddot{\theta}_1$ with f_3 in (33), we have

$$\ddddot{\mathbf{y}} = \boldsymbol{f}_3(\theta_1, \theta_{12}, \dot{\theta}_1, \dot{\theta}_{12}, u_t, \dot{u}_t, \tau, \dot{\tau}, \ddot{u}_t, u_r, \ddot{\tau}).$$

Therefore $r_1 = r_2 = r_3 = 4$ and thus $r = 12 = \bar{n}$, which means that the Condition 1 of Definition 1 is satisfied. Therefore it is now worth to analytically search for the invertibility domain of $\bar{\mathbf{G}}(\bar{\mathbf{x}})$, which is stated in the next result.

Proposition 2. *The vectors $[\mathbf{p}_c^T \ \theta_{12}]^T$, $[\mathbf{p}_m^T \ \theta_{12}]^T$ and $[\mathbf{p}_e^T \ \theta_{12}]^T$ are all exactly linearizing output via dynamic feedback for the coinciding model with rigid-joint arm (Case RC), as long as $u_t \neq 0$. As a consequence, they are also flat outputs.*

Proof. For $[\mathbf{p}_c^T \ \theta_{12}]^T$ this descends from Proposition 1 since Case RC is a special case of Case RG. Concerning $[\mathbf{p}_e^T \ \theta_{12}]^T$, this descends from (24) and from the flatness of $[\mathbf{p}_m^T \ \theta_{12}]^T$, which we shall prove in the following.

First let us write the system dynamics in the following form

$$\ddot{\mathbf{q}} = \mathbf{W} \left(\begin{array}{c} \mathbf{v} u_t - \bar{\boldsymbol{\beta}} \dot{\theta}_{12}^2 + \begin{pmatrix} 0 \\ m_s \bar{g} \end{pmatrix} \\ \hdashline \begin{pmatrix} d_{G_x} u_t + u_r - \tau \\ \tau \end{pmatrix} - \begin{pmatrix} 0 \\ g_4(\theta_{12}) \end{pmatrix} \end{array} \right), \tag{36}$$

where $\bar{\boldsymbol{\beta}} = \frac{\partial \boldsymbol{\beta}}{\theta_{12}} = [\bar{\beta}_1 \ \bar{\beta}_2]^T \in \mathbb{R}^2$, $\boldsymbol{\beta}$ as in (26), g_4 as in (28) and $\mathbf{v}$ is in (12). In this case we decompose the inverse of the inertia matrix as

$$\mathbf{W} = \mathbf{M}^{-1} = \left(\begin{array}{c:c} \mathbf{W}_{11} & \mathbf{W}_{21}^T \\ \hdashline \mathbf{W}_{21} & \mathbf{W}_{22} \end{array} \right), \mathbf{W}_{21} = \begin{pmatrix} \mathbf{0}_{1\times 2} \\ \tilde{\mathbf{W}}_{21} \in \mathbb{R}^{1\times 2} \end{pmatrix}, \tag{37}$$

where $\mathbf{W}_{11} \in \mathbb{R}^{2\times 2}$ and $\mathbf{W}_{22} = \mathrm{diag}\{W_{22^1}, W_{22^2}\} \in \mathbb{R}^{2\times 2}$. Then, we can write

$$\begin{aligned} \ddot{\mathbf{p}}_m = \mathbf{W}_{11}\mathbf{v}u_t + \tilde{\mathbf{W}}_{21}^T \tau - \\ - \mathbf{W}_{11}\bar{\boldsymbol{\beta}}\dot{\theta}_{12}^2 + \mathbf{W}_{11}\begin{pmatrix} 0 \\ m_s\bar{g} \end{pmatrix} - \tilde{\mathbf{W}}_{21}^T \mathbf{g}_4(\theta_{12}). \end{aligned} \tag{38}$$

Moreover from the third equation of (36) it is

$$\ddot{\theta}_1 = W_{22^1} u_r + W_{22^1}(d_{G_x} u_t - \tau) \tag{39}$$

and

$$\begin{aligned} \ddot{\theta}_{12} = \tilde{\mathbf{W}}_{21}\mathbf{v}u_t + W_{22^2}\tau - \\ - \tilde{\mathbf{W}}_{21}\bar{\boldsymbol{\beta}}\dot{\theta}_{12}^2 + \tilde{\mathbf{W}}_{21}\begin{pmatrix} 0 \\ m_s\bar{g} \end{pmatrix} - W_{22^2}\mathbf{g}_4(\theta_{12}). \end{aligned} \tag{40}$$

Differentiating (38) and (40) twice w.r.t. time, and utilizing $\ddot{\theta}_1$ from (39), we get

$$\begin{pmatrix} \ddddot{\mathbf{p}}_m \\ \ddddot{\theta}_{12} \end{pmatrix} = \mathbf{h}(\mathbf{q}_r, \dot{\mathbf{q}}_r, u_t, \tau, \dot{u}_t, \dot{\tau}) + \bar{\mathbf{G}}\bar{\mathbf{u}}, \tag{41}$$

where $\mathbf{q}_r$ is defined as in the proof of Proposition 1 and

$$\bar{\mathbf{G}}\bar{\mathbf{u}} = \underbrace{\left(\begin{array}{c:c:c} \mathbf{W}_{11}\mathbf{v} & \mathbf{W}_{11}\bar{\mathbf{v}}W_{22^1}u_t & \tilde{\mathbf{W}}_{21}^T \\ \hdashline \tilde{\mathbf{W}}_{21}\mathbf{v} & \tilde{\mathbf{W}}_{21}\bar{\mathbf{v}}W_{22^1}u_t & W_{22^2} \end{array} \right)}_{\bar{\mathbf{G}}} \underbrace{\begin{pmatrix} \ddot{u}_t \\ u_r \\ \ddot{\tau} \end{pmatrix}}_{\bar{\mathbf{u}}}, \tag{42}$$

[10]Notice that this inertial coupling disappears as well if the PVTOL mass is small enough, i.e. $m_1 \to 0$ (see (26)). However this is not a reasonable assumption.

[11]Notice that a particular case of this one is studied in [25], where the three points $\mathrm{P}_{\mathrm{C}_1}$, P_{G} and P_{M} are assumed to be same. In Sec. V-C we study the more general case in which P_{G} is not assumed to be coincident. Moreover in that paper, only the differential flatness was studied, while in this section we also prove the exact linearizability and provide the linearizing controller.

[12]If one develops the computations, one realizes that $\ddot{\theta}_{12}$ does not depend on $\dot{\theta}_{12}$ since the terms depending on $\dot{\theta}_{12}$ cancel out each other. However this particularity is not necessary to prove the presented result.

where $\bar{\mathbf{v}}$ is as in (13), and $\bar{\mathbf{G}}$ is the new input matrix, whose determinant can easily be computed, after some algebra, as

$$|\bar{\mathbf{G}}| = -\frac{u_t}{J_1 m_s\Big((J_2+J_m)m_s + m_2(m_1+m_m)\,\|\mathbf{d}_2\|_2^2\Big)}. \quad (43)$$

which is always invertible as long as $u_t \neq 0$. This proofs that $[\mathbf{p}_m^T\ \theta_{12}]^T$ is exact linearizing output for Case RC. From Fact 1 it is differentially flat output as well. □

Derivation of the Algebraic Map from the Flat Output

We shall show now the procedure to explicitly write down the algebraic map that relates $\ddot{\mathbf{p}}_m, \dddot{\mathbf{p}}_m, \ddddot{\mathbf{p}}_m, \theta_{12}, \dot{\theta}_{12}, \ddot{\theta}_{12}, \dddot{\theta}_{12}, \ddddot{\theta}_{12}$ with θ_1, $\dot{\theta}_1$, and $\mathbf{u}$. The position of the CoM of overall system in $\mathscr{F}_W$ is given by

$$\begin{aligned}
\mathbf{p}_c &= \mathbf{p}_m + \frac{m_2}{m_s}\mathbf{R}_{12}\mathbf{d}_2 = \mathbf{p}_c(\mathbf{y})\\
\begin{bmatrix} x_c \\ z_c \end{bmatrix} &= \begin{bmatrix} x_m + \frac{m_2}{m_s}\Big(d_{2_x}c_{12} + d_{2_z}s_{12}\Big) \\ z_m + \frac{m_2}{m_s}\Big(-d_{2_x}s_{12} + d_{2_z}c_{12}\Big) \end{bmatrix},\\
\dot{\mathbf{p}}_c &= \dot{\mathbf{p}}_m + \frac{m_2}{m_s}\bar{\mathbf{R}}_{12}\mathbf{d}_2\dot{\theta}_{12} = \mathbf{p}_c(\mathbf{y},\dot{\mathbf{y}})\\
\begin{bmatrix} \dot{x}_c \\ \dot{z}_c \end{bmatrix} &= \begin{bmatrix} \dot{x}_m + \frac{m_2\dot{\theta}_{12}}{m_s}\Big(-d_{2_x}s_{12} + d_{2_z}c_{12}\Big) \\ \dot{z}_m + \frac{m_2\dot{\theta}_{12}}{m_s}\Big(-d_{2_x}c_{12} - d_{2_z}s_{12}\Big) \end{bmatrix},\\
\ddot{\mathbf{p}}_c &= \ddot{\mathbf{p}}_m + \frac{m_2}{m_s}\Big(\bar{\mathbf{R}}_{12}\mathbf{d}_2\ddot{\theta}_{12} - \mathbf{R}_{12}\mathbf{d}_2\dot{\theta}_{12}^2\Big) = \mathbf{p}_c(\mathbf{y},\dot{\mathbf{y}},\ddot{\mathbf{y}})\\
\begin{bmatrix} \ddot{x}_c \\ \ddot{z}_c \end{bmatrix} &= \begin{bmatrix} \ddot{x}_m + \frac{m_2}{m_s}\Big(d_{2_x}(-c_{12}\dot{\theta}_{12}^2 - s_{12}\ddot{\theta}_{12}) + d_{2_z}(-s_{12}\dot{\theta}_{12}^2 + c_{12}\ddot{\theta}_{12})\Big) \\ \ddot{z}_m + \frac{m_2}{m_s}\Big(d_{2_x}(s_{12}\dot{\theta}_{12}^2 - c_{12}\ddot{\theta}_{12}) + d_{2_z}(-c_{12}\dot{\theta}_{12}^2 - s_{12}\ddot{\theta}_{12})\Big) \end{bmatrix},
\end{aligned} \quad (44)$$

where $s_* = \sin(\theta_*)$ and $c_* = \cos(\theta_*)$. The computation of u_t and θ_1 is exactly as in Case RG. Hence substituting (44) in (21) and in (22), we find $u_t, \dot{u}_t, \ddot{u}_t$ and $\theta_1, \dot{\theta}_1, \ddot{\theta}_1$ as functions of $\mathbf{y}, \cdots, \ddddot{\mathbf{y}}$. Furthermore, the motor torque can be retrieved from the last equation of the system dynamics as

$$\tau = \tau(\theta_{12}, \ddot{\mathbf{p}}_m, \ddot{\theta}_{12}) = \boldsymbol{\beta}^T(\theta_{12})\ddot{\mathbf{p}}_m + m_B\ddot{\theta}_{12} + g_4(\theta_{12}). \quad (45)$$

Now, noticing that (from (28)) $g_4(\theta_{12}) = -\boldsymbol{\beta}(\theta_{12})\bar{g}\cdot\mathbf{e}_2$ with $\mathbf{e}_2 = [0\ 1]^T \in \mathbb{R}^2$, and $\cdot$ being the *dot-product*, and recalling that $\bar{\boldsymbol{\beta}} = \frac{\partial \boldsymbol{\beta}}{\partial \theta_{12}}$, we can write

$$\begin{aligned}
\dot{\tau} &= \boldsymbol{\beta}^T\dddot{\mathbf{p}}_m + m_B\dddot{\theta}_{12} + (\bar{\boldsymbol{\beta}}^T\ddot{\mathbf{p}}_m - \bar{\boldsymbol{\beta}}\bar{g}\cdot\mathbf{e}_2)\dot{\theta}_{12}\\
\ddot{\tau} &= \boldsymbol{\beta}^T\ddddot{\mathbf{p}}_m + m_B\ddddot{\theta}_{12} + 2\bar{\boldsymbol{\beta}}^T\dddot{\mathbf{p}}_m\dot{\theta}_{12} +\\
&\quad + (\bar{\boldsymbol{\beta}}^T\ddot{\mathbf{p}}_m - \bar{\boldsymbol{\beta}}\bar{g}\cdot\mathbf{e}_2)\ddot{\theta}_{12} + (\boldsymbol{\beta}\bar{g}\cdot\mathbf{e}_2 - \boldsymbol{\beta}^T\ddot{\mathbf{p}}_m)\dot{\theta}_{12}^2,
\end{aligned} \quad (46)$$

which means $\dot{\tau} = \dot{\tau}(\mathbf{y},\dot{\mathbf{y}},\ddot{\mathbf{y}},\dddot{\mathbf{y}})$, and $\ddot{\tau} = \ddot{\tau}(\mathbf{y},\dot{\mathbf{y}},\ddot{\mathbf{y}},\dddot{\mathbf{y}},\ddddot{\mathbf{y}})$.

Then, using the third row of the system dynamics, we obtain

$$u_r = u_r(\ddot{\theta}_1, u_t, \tau) = J_1\ddot{\theta}_1 + \tau - d_{G_x}u_t, \quad (47)$$

where by knowing τ from (45), and utilizing $\ddot{\theta}_1$ from (22) and u_t from (21), and taking (44) into consideration, we have that $u_r = u_r(\mathbf{y},\dot{\mathbf{y}},\ddot{\mathbf{y}},\dddot{\mathbf{y}},\ddddot{\mathbf{y}})$.

In summary, we have obtained $\mathbf{p}_m = \mathbf{p}_m(\mathbf{y})$, $\dot{\mathbf{p}}_m = \dot{\mathbf{p}}_m(\dot{\mathbf{y}})$, $\ddot{\mathbf{p}}_c = \ddot{\mathbf{p}}_m(\ddot{\mathbf{y}})$ and $\theta_{12} = \theta_{12}(\mathbf{y})$, $\dot{\theta}_{12} = \dot{\theta}_{12}(\dot{\mathbf{y}})$, $\ddot{\theta}_{12} = \ddot{\theta}_{12}(\ddot{\mathbf{y}})$ from the definition; $u_t = u_t(\mathbf{y},\dot{\mathbf{y}},\ddot{\mathbf{y}})$, $\dot{u}_t = \dot{u}_t(\mathbf{y},\dot{\mathbf{y}},\ddot{\mathbf{y}},\dddot{\mathbf{y}})$, $\ddot{u}_t = \ddot{u}_t(\mathbf{y},\dot{\mathbf{y}},\ddot{\mathbf{y}},\dddot{\mathbf{y}},\ddddot{\mathbf{y}})$ from (21) and $\theta_1 = \theta_1(\mathbf{y},\dot{\mathbf{y}},\ddot{\mathbf{y}})$, $\dot{\theta}_1 = \dot{\theta}_1(\mathbf{y},\dot{\mathbf{y}},\ddot{\mathbf{y}},\dddot{\mathbf{y}})$, $\ddot{\theta}_1 = \ddot{\theta}_1(\mathbf{y},\dot{\mathbf{y}},\ddot{\mathbf{y}},\dddot{\mathbf{y}},\ddddot{\mathbf{y}})$ from (22) where for both $\mathbf{p}_c$ is computed from (44); and finally $\tau = \tau(\mathbf{y},\ddot{\mathbf{y}})$, $\dot{\tau} = \dot{\tau}(\mathbf{y},\dot{\mathbf{y}},\ddot{\mathbf{y}},\dddot{\mathbf{y}})$, $\ddot{\tau} = \ddot{\tau}(\mathbf{y},\dot{\mathbf{y}},\ddot{\mathbf{y}},\dddot{\mathbf{y}},\ddddot{\mathbf{y}})$ from (45)-(46), and $u_r = u_r(\mathbf{y},\dot{\mathbf{y}},\ddot{\mathbf{y}},\dddot{\mathbf{y}},\ddddot{\mathbf{y}})$ from (47). Hence we showed how to compute the states and the control inputs of the system as functions of the flat outputs and their finite number of derivatives.

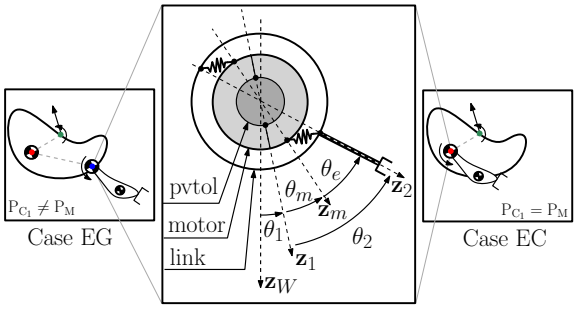


Fig. 3: An example of elastic-joint between the motor shaft and the link attached to PVTOL. The motor is magnified w.r.t. the PVTOL considering both the EG and the EC cases. The innermost circle is fixed in $\mathscr{F}_1$, thus rigidly attached to the PVTOL. The middle circle is rigidly attached to the motor output shaft, i.e., fixed in $\mathscr{F}_M$. The outermost circle is connected to the middle circle via some elastic components, and it is rigidly connected to the link, thus fixed in $\mathscr{F}_2$.

VI. PVTOL with an Elastic–Joint Arm

A. Elastic-Joint Attached to a Generic Point (EG case)

In this section we consider the model of the PVTOL given in Fig. 1, with an elastic joint between the motor output shaft and the arm link. A sketch of such connection is shown in Fig. 3. This case is referred to as Case EG in Table I. The number of generalized coordinates for this case is increased by one with respect to the RG case ($n = 5$) due to the fact that the output shaft of the motor and the link are not rigidly connected and therefore two distinct coordinates are needed to describe the system configuration, namely θ_{1m} and θ_{12}.

In order to keep the translational dynamics decoupled from the rotational one let us chose as generalized coordinates $\mathbf{q} = [\mathbf{p}_c^T\ \theta_1\ \theta_{12}\ \theta_{1m}]^T \in \mathbb{R}^5$. Notice that, differently from the rigid-joint cases (Case RG and Case RC), we have $\theta_2 \neq \theta_m$. In fact $\theta_2 = \theta_m + \theta_e$ (see Fig. 1 and Fig. 3). Whenever $\theta_e = \theta_2 - \theta_m = \theta_{12} - \theta_{1m}$ is nonzero the elastic link is deflected and stores elastic potential energy.

After some algebra it is possible to compute the matrices and vectors in (1) for this case. The inertia matrix is

$$\mathbf{M} = \begin{pmatrix} m_s\mathbf{I}_2 & * & * & * \\ \mathbf{0}_{1\times 2} & m_a & * & * \\ \mathbf{0}_{1\times 2} & m_{ab}(\theta_1,\theta_{12}) & m_b - J_m & * \\ \mathbf{0}_{1\times 2} & 0 & 0 & J_m \end{pmatrix} = \mathbf{M}^T \in \mathbb{R}^{5\times 5}, \quad (48)$$

where $m_a\, m_b$ and m_{ab} are given in (8). The centrifugal/Coriolis and gravitational forces are

$$\mathbf{c}(\mathbf{q},\dot{\mathbf{q}}) = \begin{bmatrix} 0 \\ 0 \\ \frac{m_1 m_2}{m_s}\mathbf{d_1}^T\bar{\mathbf{R}}_2\mathbf{d_2}\dot{\theta}_{12}^2 \\ -\frac{m_1 m_2}{m_s}\mathbf{d_1}^T\bar{\mathbf{R}}_2\mathbf{d_2}\dot{\theta}_1^2 \\ 0 \end{bmatrix}, \quad \mathbf{g} = \begin{bmatrix} 0 \\ -m_s\bar{g} \\ 0 \\ 0 \\ 0 \end{bmatrix}, \quad (49)$$

the control input matrix $\mathbf{G}$ and the elastic forces $\mathbf{f}_E$ due to the elastic potential energy are

$$\mathbf{G}(\mathbf{q}) = \begin{pmatrix} g_{11} & 0 & 0 \\ g_{21} & 0 & 0 \\ g_{31} & 1 & -1 \\ g_{41} & 0 & 0 \\ 0 & 0 & 1 \end{pmatrix}, \quad \mathbf{f}_E(\mathbf{q}) = \begin{bmatrix} 0 \\ 0 \\ 0 \\ f_l(\theta_{1m},\theta_{12}) \\ f_m(\theta_{1m},\theta_{12}) \end{bmatrix}, \tag{50}$$

where $[g_{11}\ g_{21}\ g_{31}\ g_{41}]^T$ is as the first column of $\mathbf{G}$ in (10). Notice that $f_l(\theta_{1m},\theta_{12})$ is the elastic force acting on the link side, and $f_m(\theta_{1m},\theta_{12})$ is the elastic force acting on the motor side. These forces can be nonlinear functions of θ_{1m} and θ_{12}. In the linear spring case, $f_l(\theta_{1m},\theta_{12}) = k_e(\theta_{1m}-\theta_{12})$ and $f_m(\theta_{1m},\theta_{12}) = k_e(\theta_{12}-\theta_{1m})$, where $k_e > 0$ is the stiffness of the elastic element.

Writing down the dependences of $\ddot{\mathbf{q}}$ for this case we obtain

$$\begin{aligned} \ddot{x}_c &= f_1(\theta_1,u_t), \quad \ddot{z}_c = f_2(\theta_1,u_t) \\ \ddot{\theta}_1 &= f_3(\theta_1,\theta_{12},\theta_{1m},\dot{\theta}_1,\dot{\theta}_{12},u_t,u_r,\tau) \\ \ddot{\theta}_{12} &= f_4(\theta_1,\theta_{12},\theta_{1m},\dot{\theta}_1,\dot{\theta}_{12},u_t,u_r,\tau) \\ \ddot{\theta}_{1m} &= f_6(\theta_{12},\theta_{1m},\tau). \end{aligned} \tag{51}$$

As we can see, a part from the introduction of θ_{1m} the dependency on the other coordinates is the same as the one in (11) for Case RG. However, the fact that $n=5$ (instead of 4) makes the solution adopted for Case RG not immediately applicable. In fact if we set, as in Section V-A, $s_1 = 2$, $s_2 = s_3 = 0$ and we check whether Condition 1 of Definition 1 is satisfied for the output $[\mathbf{p}_c^T\ \theta_{12}]^T$ we fail, since we obtain $\bar{n} = 2n+s_1 = 10+2 = 12$ (instead of $\bar{n} = 2n+s_1 = 8+2 = 10$) and $r = 10$ (as in Case RG). Therefore it is not straightforward to find the exactly linearizing (flat) output for this case. The reason is that this time we do not gain enough relative degree to reach the new $\bar{n} = 12$. A way to gain more relative degree would be to let $\ddot{\theta}_{12}$ depend on less inputs, since right now is depending on all the inputs. The reason for this dependency is the strong inertial coupling between θ_1 and θ_{12}, see (48). Therefore in the following we try whether is possible in some way to loosen this coupling in order to let less inputs appear in $\ddot{\theta}_{12}$.

In order to take a closer look to the rotational coupling let us consider for a moment only the orientation dynamics:

$$\begin{aligned} \begin{bmatrix} \ddot{\theta}_1 \\ \ddot{\theta}_{12} \end{bmatrix} &= \mathbf{B}^{-1} \begin{bmatrix} g_{31}u_t - c_3(\theta_1,\theta_{12},\dot{\theta}_{12}) + u_r - \tau \\ g_{41}(\theta_1,\theta_{12})u_t + f_l(\theta_{1m},\theta_{12}) - c_4(\theta_1,\theta_{12},\dot{\theta}_1) \end{bmatrix} \\ \ddot{\theta}_{1m} &= J_m^{-1}\Big(f_m(\theta_{1m},\theta_{12}) + \tau\Big) \end{aligned} \tag{52}$$

with

$$\mathbf{B} = \begin{pmatrix} m_a & m_{ab} \\ m_{ab} & m_b - J_m \end{pmatrix}, \begin{bmatrix} c_3 \\ c_4 \end{bmatrix} = \begin{bmatrix} \frac{m_1 m_2}{m_s}\mathbf{d_1}^T\bar{\mathbf{R}}_2\mathbf{d_2}\dot{\theta}_{12}^2 \\ -\frac{m_1 m_2}{m_s}\mathbf{d_1}^T\bar{\mathbf{R}}_2\mathbf{d_2}\dot{\theta}_1^2 \end{bmatrix}. \tag{53}$$

This orientation dynamics shares some similarities with the model of a *grounded* planar robot with mixed rigid/elastic joints. It is as if a 'virtual ground base' and the PVTOL are connected through a rigid joint to which it is applied the torque $u_r - \tau$, and the PVTOL and the link are connected through an elastic joint that is actuated by the motor torque τ. However the models are not the same because, e.g., of the the presence of the terms multiplying u_t.

Mixed rigid/elastic-joints arms for *grounded* manipulators have been studied in [33] where the author showed that it is possible to have input-output decoupling and full state linearization for such system, even if there are inertial couplings as in matrix B given in (53), based on dynamic state feedback. Shortly, this is done with a linear dynamic feedback compensator defined for the rigid joint, which let it behave as a *fictitious* elastic joint transmission. To be best of our knowledge this kind of method has never been used for *aerial* manipulators, whose base are (differently from [33]) floating and underactuated.

First, let us extend the systems with two new states, θ_r and $\dot{\theta}_r$ and consider the following dynamic compensator

$$\begin{aligned} u_r - \tau &= k_r(\theta_r - \theta_1) \\ J_r\ddot{\theta}_r + k_r(\theta_r - \theta_1) &= u_n, \end{aligned} \tag{54}$$

where $k_r \in \mathbb{R}_{>0}$ and $J_r \in \mathbb{R}_{>0}$ are two additional systems parameters, and u_n is a new control input that replaces u_r. Now, replacing $u_r - \tau$ in first equation of (52) with the first equation of (54), we have

$$\begin{aligned} \begin{bmatrix} \ddot{\theta}_1 \\ \ddot{\theta}_{12} \end{bmatrix} &= \mathbf{B}^{-1} \begin{bmatrix} g_{31}u_t + k_r(\theta_r - \theta_1) - c_3(\theta_1,\theta_{12},\dot{\theta}_{12}) \\ g_{41}(\theta_1,\theta_{12})u_t + f_l(\theta_{1m},\theta_{12}) - c_4(\theta_1,\theta_{12},\dot{\theta}_1) \end{bmatrix} \\ \begin{bmatrix} \ddot{\theta}_r \\ \ddot{\theta}_{1m} \end{bmatrix} &= \begin{pmatrix} J_r & 0 \\ 0 & J_m \end{pmatrix}^{-1} \begin{bmatrix} k_r(\theta_1 - \theta_r) + u_n \\ f_m(\theta_{1m},\theta_{12}) + \tau \end{bmatrix}. \end{aligned} \tag{55}$$

Putting back in place the translational dynamics and writing down the dependences of $\ddot{\mathbf{q}}$ including the new states of the compensator (i.e., considering $\mathbf{q} = [\mathbf{p}_c^T\ \theta_1\ \theta_{12}\ \theta_r\ \theta_{1m}]^T \in \mathbb{R}^6$) we obtain

$$\begin{aligned} \ddot{x}_c &= f_1(\theta_1,u_t), \quad \ddot{z}_c = f_2(\theta_1,u_t) \\ \ddot{\theta}_1 &= f_3(\theta_1,\theta_{12},\theta_{1m},\theta_r,\dot{\theta}_1,\dot{\theta}_{12},u_t) \\ \ddot{\theta}_{12} &= f_4(\theta_1,\theta_{12},\theta_{1m},\theta_r,\dot{\theta}_1,\dot{\theta}_{12},u_t) \\ \ddot{\theta}_r &= f_5(\theta_1,\theta_r,u_n), \quad \ddot{\theta}_{1m} = f_6(\theta_{12},\theta_{1m},\tau). \end{aligned} \tag{56}$$

Notice that with the introduction of the compensator the number of states has become $2n = 12$. However, thanks to the compensation applied above, $\ddot{\theta}_{12}$ does not directly depend on u_r and τ anymore. Therefore there is hope that if we choose as new input a high order derivative of u_t then the the relative degree will be enough this time to let the output $\mathbf{y} = [\mathbf{p}_c^T\ \theta_{12}]^T = [\mathbf{y}_1^T\ y_2]^T$ satisfy Condition 1 of Definition 1.

Let us consider then $s_1 = 4$, $s_2 = s_3 = 0$. With this choice we have $\bar{n} = 2n+4 = 16$. We then obtain as new control inputs[13] $\bar{\mathbf{u}} = [\dddot{u}_t\ u_n\ \tau]^T \in \mathbb{R}^3$ and the new state $\bar{\mathbf{x}} = [\mathbf{q}^T\ \dot{\mathbf{q}}^T\ u_t\ \dot{u}_t\ \ddot{u}_t\ \dddot{u}_t]^T \in \mathbb{R}^{16}$. The functional dependency of the derivatives of $\mathbf{y}_1$ can be written as follows

$$\ddot{\mathbf{y}}_1 = (f_1\ f_2)^T = \boldsymbol{\xi}_1(\theta_1,u_t), \quad \dddot{\mathbf{y}}_1 = \boldsymbol{\xi}_2(\theta_1,\dot{\theta}_1,u_t,\dot{u}_t) \tag{57}$$

considering that both $\ddot{\theta}_1$ and $\ddot{\theta}_{12}$ are available from (56), we can write

$$\begin{aligned} \ddddot{\mathbf{y}} &= \boldsymbol{\xi}_3(\theta_1,\theta_{12},\theta_{1m},\theta_r,\dot{\theta}_1,\dot{\theta}_{12},u_t,\dot{u}_t,\ddot{u}_t) \\ \mathbf{y}_1^{(5)} &= \boldsymbol{\xi}_4(\theta_1,\theta_{12},\theta_{1m},\theta_r,\dot{\theta}_1,\dot{\theta}_{12},\dot{\theta}_{1m},\dot{\theta}_r,u_t,\dot{u}_t,\ddot{u}_t,\dddot{u}_t) \end{aligned} \tag{58}$$

and using $\ddot{\theta}_r$ and $\ddot{\theta}_{1m}$ from (56), we can write

$$\begin{aligned} \mathbf{y}_1^{(6)} = \boldsymbol{\xi}_5(&\theta_1,\theta_{12},\theta_{1m},\theta_r,\dot{\theta}_1,\dot{\theta}_{12},\dot{\theta}_{1m},\dot{\theta}_r,u_t,\dot{u}_t,\ddot{u}_t,\dddot{u}, \\ &,\ddddot{u}_t,u_n,\tau), \end{aligned}$$

[13] Notice that once τ and u_n are computed, u_r can be calculated using (54).

where we stop because $\dddot{u}$, u_n, and τ appear now linearly in $\mathbf{y}_1^{(6)}$. Therefore we have that $r_1 = r_2 = 6$.

In the same fashion, we can write the derivatives of y_2 as

$$\ddot{y}_2 = f_4 = \mu_1(\theta_1, \theta_{12}, \theta_{1m}, \theta_r, \dot{\theta}_1, \dot{\theta}_{12}, u_t) \tag{59}$$

and, considering that $\ddot{\theta}_1$ and $\ddot{\theta}_{12}$ are available from (56)

$$\dddot{y}_2 = \mu_2(\theta_1, \theta_{12}, \theta_{1m}, \theta_r, \dot{\theta}_1, \dot{\theta}_{12}, \dot{\theta}_{1m}, \dot{\theta}_r, u_t, \dot{u}_t) \tag{60}$$

and using $\ddot{\theta}_r$ and $\ddot{\theta}_{1m}$ from (56), we can write

$$\ddddot{y}_2 = \mu_3(\theta_1, \theta_{12}, \theta_{1m}, \theta_r, \dot{\theta}_1, \dot{\theta}_{12}, \dot{\theta}_{1m}, \dot{\theta}_r, u_t, \dot{u}_t, \ddot{u}_t, u_n, \tau).$$

Therefore $r_3 = 4$ and $r_1 + r_2 + r_3 = 16 = \bar{n}$, which means that the Condition 1 of Definition 1 is satisfied. Therefore it is now worth to analytically search for the invertibility domain of $\bar{\mathbf{G}}(\bar{\mathbf{x}})$, which is done in the next result.

Proposition 3. *The vector $[\mathbf{p}_c^T \ \theta_{12}]^T$ is an exactly linearizing output via dynamic feedback for the generic model with an elastic-joint arm (Case EG), as long as $u_t \neq 0$, $k_r \neq 0$ and $k_e \neq 0$ (if the elasticity is linear). As a consequence, it is also a flat output.*

Proof. Let us re-formalize the system dynamics given in (56) (assuming linear spring case) as

$$m_s \ddot{\mathbf{p}}_c = \mathbf{v} u_t + \begin{pmatrix} 0 \\ m_s \bar{g} \end{pmatrix}, \quad \mathbf{v} = \begin{pmatrix} -\sin(\theta_1) \\ -\cos(\theta_1) \end{pmatrix} \in \mathbb{R}^2 \tag{61a}$$

$$\begin{bmatrix} \ddot{\theta}_1 \\ \ddot{\theta}_{12} \end{bmatrix} = \mathbf{W} \begin{bmatrix} g_{31} u_t + k_r(\theta_r - \theta_1) - c_3(\theta_1, \theta_{12}, \dot{\theta}_{12}) \\ g_{41}(\theta_1, \theta_{12}) u_t + k_e(\theta_{1m} - \theta_{12}) - c_4(\theta_1, \theta_{12}, \dot{\theta}_1) \end{bmatrix} \tag{61b}$$

$$\begin{bmatrix} \ddot{\theta}_r \\ \ddot{\theta}_{1m} \end{bmatrix} = \begin{pmatrix} J_r & 0 \\ 0 & J_m \end{pmatrix}^{-1} \begin{bmatrix} k_r(\theta_1 - \theta_r) + u_n \\ k_e(\theta_{12} - \theta_{1m}) + \tau \end{bmatrix}, \tag{61c}$$

where this time $\mathbf{q}_r = [\theta_1 \ \theta_{12} \ \theta_r \ \theta_{1m}]^T \in \mathbb{R}^4$ and $\mathbf{W} = \mathbf{B}^{-1}$. In the following, by W_{ij}, we denote the ij-th component of $\mathbf{W}$.

Then differentiating (61a) four times w.r.t. the time, we get

$$m_s \mathbf{p}_c^{(6)} = \mathbf{v} \dddot{u}_t + \bar{\mathbf{v}} u_t \ddddot{\theta}_1 + \mathbf{h}_1(\mathbf{q}_r, \dot{\mathbf{q}}_r, u_t, \dot{u}_t, \ddot{u}_t, \dddot{u}_t). \tag{62}$$

The quantity $\ddddot{\theta}_1$ can be analytically expressed by differentiating twice $\ddot{\theta}_1$, whose analytical expression is available from the first equation of (61b), substituting: $\ddot{\theta}_{12}$ from the second equation of (61b), $\ddot{\theta}_r$, and $\ddot{\theta}_{1m}$ from (61c). In this way we obtain

$$\ddddot{\theta}_1 = \frac{W_{11} k_r}{J_r} u_n + \frac{W_{12} k_e}{J_m} \tau + h_2(\mathbf{q}_r, \dot{\mathbf{q}}_r, u_t, \dot{u}_t, \ddot{u}_t) \tag{63}$$

and utilizing it in (62), we have

$$\mathbf{p}_c^{(6)} = \frac{\mathbf{v}}{m_s} \dddot{u}_t + \bar{\mathbf{v}} u_t \frac{W_{11} k_r}{m_s J_r} u_n + \bar{\mathbf{v}} u_t \frac{W_{12} k_e}{m_s J_m} \tau + \\ + \mathbf{h}_A(\mathbf{q}_r, \dot{\mathbf{q}}_r, u_t, \dot{u}_t, \ddot{u}_t, \dddot{u}_t), \tag{64}$$

where $\mathbf{h}_A = \mathbf{h}_1 + \bar{\mathbf{v}} u_t h_2 \in \mathbb{R}^{2\times 1}$ and $\bar{\mathbf{v}}$ is as in (13).

Similarly, we express analytically $\ddddot{\theta}_{12}$ by differentiating twice $\ddot{\theta}_{12}$ and substituting $\ddot{\theta}_r$ and $\ddot{\theta}_{1m}$ using (61), thus getting

$$\ddddot{\theta}_{12} = \frac{W_{12} k_r}{J_r} u_n + \frac{W_{22} k_e}{J_m} \tau + h_b(\mathbf{q}_r, \dot{\mathbf{q}}_r, u_t, \dot{u}_t, \ddot{u}_t). \tag{65}$$

Then, using (64) and (65) we can write

$$\begin{pmatrix} \mathbf{p}_c^{(6)} \\ \ddddot{\theta}_{12} \end{pmatrix} = \mathbf{h}(\mathbf{q}_r, \dot{\mathbf{q}}_r, u_t, \dot{u}_t, \ddot{u}_t, \dddot{u}_t) + \bar{\mathbf{G}} \bar{\mathbf{u}}, \tag{66}$$

where $\mathbf{h} = [\mathbf{h}_A \ h_b]^T \in \mathbb{R}^{3\times 1}$ and

$$\bar{\mathbf{G}}\bar{\mathbf{u}} = \underbrace{\left(\begin{array}{c:c:c} \frac{\mathbf{v}}{m_s} & u_t \bar{\mathbf{v}} \frac{W_{11} k_r}{m_s J_r} & u_t \bar{\mathbf{v}} \frac{W_{12} k_e}{m_s J_m} \\ \hdashline 0 & \frac{W_{12} k_r}{J_r} & \frac{W_{22} k_e}{J_m} \end{array}\right)}_{\bar{\mathbf{G}}} \underbrace{\begin{pmatrix} \dddot{u}_t \\ u_n \\ \tau \end{pmatrix}}_{\bar{\mathbf{u}}}, \tag{67}$$

where $\bar{\mathbf{G}}$ is sought input matrix (remember that $u_r = u_n - \tau$). The determinant of $\bar{\mathbf{G}}$ is

$$|\bar{\mathbf{G}}| = -\frac{u_t k_r k_e (W_{11} W_{22} - W_{12}^2)}{J_m J_r m_s^2} = -\frac{u_t k_r k_e |\mathbf{W}|}{J_m J_r m_s^2} \\ = -\frac{u_t k_r k_e}{J_m J_r m_s^2 |\mathbf{B}|}. \tag{68}$$

By construction it is always $J_m J_r m_s^2 > 0$, in order to show that the determinant is well defined we now show that it is also $|\mathbf{B}| > 0$. In fact we have:

$$|\mathbf{B}| = m_a m_b - m_{ab}^2 - m_a J_m \\ = m_{pos2} + m_\alpha m_\beta (\mathbf{d}_\alpha^T \mathbf{d}_\alpha)(\mathbf{d}_\beta^T \mathbf{d}_\beta) - m_\gamma^2 (\mathbf{d}_\alpha^T \mathbf{d}_\beta)(\mathbf{d}_\alpha^T \mathbf{d}_\beta), \tag{69}$$

where $m_{pos2} = m_\alpha J_2 \mathbf{d}_\alpha^T \mathbf{d}_\alpha + m_\beta J_1 \mathbf{d}_\beta^T \mathbf{d}_\beta + J_1 J_2 > 0$. Moreover, $(\mathbf{d}_\alpha^T \mathbf{d}_\alpha)(\mathbf{d}_\beta^T \mathbf{d}_\beta) - (\mathbf{d}_\alpha^T \mathbf{d}_\beta)(\mathbf{d}_\alpha^T \mathbf{d}_\beta) = (d_{\alpha_1} d_{\beta_2} - d_{\alpha_2} d_{\beta_1})^2 > 0$ and it is always $(\mathbf{d}_\alpha^T \mathbf{d}_\alpha)(\mathbf{d}_\beta^T \mathbf{d}_\beta) > 0$, where d_{α_i} and $d_{\beta i}$ are the i-th components of $\mathbf{d}_\alpha$ and $\mathbf{d}_\beta$, respectively. Hence we have that $|\mathbf{B}| > 0$.

Since the denominator in (68) is always positive the matrix $\bar{\mathbf{G}}$ is invertible as long as $u_t \neq 0$, $k_r \neq 0$, $J_r \neq 0$ and $k_e \neq 0$ (if the elasticity is linear). This proofs that $[\mathbf{p}_c^T \ \theta_{12}]^T$ is exact linearizing output for Case EG. From Fact 1 it is differentially flat output as well. □

Derivation of the Algebraic Map from the Flat Output

We shall now show how to explicitly write down the algebraic map that relates $\ddot{\mathbf{p}}_c, \dddot{\mathbf{p}}_c, \ddddot{\mathbf{p}}_c, \mathbf{p}_c^{(5)}, \mathbf{p}_c^{(6)}, \theta_{12}, \dot{\theta}_{12}, \ddot{\theta}_{12}, \dddot{\theta}_{12}, \ddddot{\theta}_{12}$ with θ_1, $\dot{\theta}_1$, θ_{1m}, $\dot{\theta}_{1m}$, and $\mathbf{u}$.

Similar to the RG case, it is clear from the system dynamics that we can retrieve $u_t, \dot{u}_t, \ddot{u}_t$ and $\theta_1, \dot{\theta}_1, \ddot{\theta}_1$ from (21) and (22), respectively. Furthermore, θ_{1m} can be solved from the fourth equation of the system dynamics as

$$\theta_{1m} = \theta_{1m}(\theta_{12}, \ddot{\theta}_{12}, \theta_1, \dot{\theta}_1, \ddot{\theta}_1, u_t) = \frac{1}{k_e} \Big(m_{ab}(\theta_1, \theta_{12}) \ddot{\theta}_1 + \\ + (m_b - J_m) \ddot{\theta}_{12} + c_4(\theta_1, \theta_{12}, \dot{\theta}_1) + k_e \theta_{12} - g_{41}(\theta_1, \theta_{12}) u_t \Big), \tag{70}$$

where c_4 is the fourth row of $\mathbf{c}$ given in (49). By introducing $\theta_1 = \theta_1(\ddot{\mathbf{y}}_1)$, $\dot{\theta}_1 = \dot{\theta}_1(\ddot{\mathbf{y}}_1, \dddot{\mathbf{y}}_1)$, $\ddot{\theta}_1 = \ddot{\theta}_1(\ddot{\mathbf{y}}_1, \dddot{\mathbf{y}}_1, \ddddot{\mathbf{y}}_1)$ from (22) and u_t from (21) we can show that $\theta_{1m} = \theta_{1m}(\ddot{\mathbf{y}}_1, \dddot{\mathbf{y}}_1, \ddddot{\mathbf{y}}_1, y_2, \ddot{y}_2)$, and this implies: $\dot{\theta}_{1m} = \dot{\theta}_{1m}(\ddot{\mathbf{y}}_1, \dddot{\mathbf{y}}_1, \ddddot{\mathbf{y}}_1, \mathbf{y}^{(5)}, y_2, \dot{y}_2, \ddot{y}_2, \dddot{y}_2)$ and

$\ddot{\theta}_{1m} = \ddot{\theta}_{1m}(\ddot{\mathbf{y}}_1, \dddot{\mathbf{y}}_1, \ddddot{\mathbf{y}}_1, \mathbf{y}^{(5)}, \mathbf{y}^{(6)}, y_2, \dot{y}_2, \ddot{y}_2, \dddot{y}_2, \ddddot{y}_2)$[14]. The motor torque is obtained from the fifth equation of the system dynamics, i.e.

$$\tau = J_m \ddot{\theta}_{1m} + k_e \theta_{1m} - k_e \theta_{12}, \tag{71}$$

where substituting θ_{1m} and $\ddot{\theta}_{1m}$ using (70), we can show that $\tau = \tau(\ddot{\mathbf{y}}_1, \dddot{\mathbf{y}}_1, \ddddot{\mathbf{y}}_1, \mathbf{y}^{(5)}, \mathbf{y}^{(6)}, y_2, \dot{y}_2, \ddot{y}_2, \dddot{y}_2, \ddddot{y}_2)$. Finally solving u_r from the third equation of the system dynamics, one obtains

$$u_r = u_r(\theta_{12}, \dot{\theta}_{12}, \ddot{\theta}_{12}, \theta_1, \ddot{\theta}_1, u_t, \tau) = m_a \ddot{\theta}_1 + m_{ab}(\theta_1, \theta_{12}) \ddot{\theta}_{12} + \\ + \frac{m_1 m_2}{m_s} \mathbf{d_1}^T \bar{\mathbf{R}}_2(\theta_1, \theta_{12}) \mathbf{d_2} \dot{\theta}_{12}^2 + \tau - g_{31} u_t, \tag{72}$$

where utilizing $\theta_1, \dot{\theta}_1, \ddot{\theta}_1$ from (22), u_t from (21), and τ from (71) we obtain $u_r = u_r(\ddot{\mathbf{y}}_1, \dddot{\mathbf{y}}_1, \ddddot{\mathbf{y}}_1, \mathbf{y}^{(5)}, \mathbf{y}^{(6)}, y_2, \dot{y}_2, \ddot{y}_2, \dddot{y}_2, \ddddot{y}_2)$.

In summary, we have $\mathbf{p}_c = \mathbf{y}_1$, $\dot{\mathbf{p}}_c = \dot{\mathbf{y}}_1$, $\ddot{\mathbf{p}}_c = \ddot{\mathbf{y}}_1$ and $\theta_{12} = y_2$, $\dot{\theta}_{12} = \dot{y}_2$, $\ddot{\theta}_{12} = \ddot{y}_2$ from the definition; $u_t = u_t(\ddot{\mathbf{y}}_1)$, $\dot{u}_t = \dot{u}_t(\ddot{\mathbf{y}}_1, \dddot{\mathbf{y}}_1)$, $\ddot{u}_t = \ddot{u}_t(\ddot{\mathbf{y}}_1, \dddot{\mathbf{y}}_1, \ddddot{\mathbf{y}}_1)$ from (21); $\theta_1 = \theta_1(\ddot{\mathbf{y}}_1)$, $\dot{\theta}_1 = \dot{\theta}_1(\ddot{\mathbf{y}}_1, \dddot{\mathbf{y}}_1)$, $\ddot{\theta}_1 = \ddot{\theta}_1(\ddot{\mathbf{y}}_1, \dddot{\mathbf{y}}_1, \ddddot{\mathbf{y}}_1)$ from (22); $\theta_{1m} = \theta_{1m}(\ddot{\mathbf{y}}_1, \dddot{\mathbf{y}}_1, \ddddot{\mathbf{y}}_1, y_2, \ddot{y}_2)$, $\dot{\theta}_{1m} = \dot{\theta}_{1m}(\ddot{\mathbf{y}}_1, \dddot{\mathbf{y}}_1, \ddddot{\mathbf{y}}_1, \mathbf{y}^{(5)}, y_2, \dot{y}_2, \ddot{y}_2, \dddot{y}_2)$, and $\ddot{\theta}_{1m} = \ddot{\theta}_{1m}(\ddot{\mathbf{y}}_1, \dddot{\mathbf{y}}_1, \ddddot{\mathbf{y}}_1, \mathbf{y}^{(5)}, \mathbf{y}^{(6)}, y_2, \dot{y}_2, \ddot{y}_2, \dddot{y}_2, \ddddot{y}_2)$ using (70); $\tau = \tau(\ddot{\mathbf{y}}_1, \dddot{\mathbf{y}}_1, \ddddot{\mathbf{y}}_1, \mathbf{y}^{(5)}, \mathbf{y}^{(6)}, y_2, \dot{y}_2, \ddot{y}_2, \dddot{y}_2, \ddddot{y}_2)$ from (71) and finally $u_r = u_r(\ddot{\mathbf{y}}_1, \dddot{\mathbf{y}}_1, \ddddot{\mathbf{y}}_1, \mathbf{y}^{(5)}, \mathbf{y}^{(6)}, y_2, \dot{y}_2, \ddot{y}_2, \dddot{y}_2, \ddddot{y}_2)$ from (72). Moreover, one can see that $\dddot{u}_t = \dddot{u}_t(\ddot{\mathbf{y}}_1, \dddot{\mathbf{y}}_1, \ddddot{\mathbf{y}}_1, \mathbf{y}_1^{(5)})$, $\ddddot{u}_t = \ddddot{u}_t(\ddot{\mathbf{y}}_1, \dddot{\mathbf{y}}_1, \ddddot{\mathbf{y}}_1, \mathbf{y}_1^{(5)}, \mathbf{y}_1^{(6)})$ using (21). Hence we showed the states and the control inputs of the system as functions of the flat outputs and their finite number of derivatives.

B. Elastic-joint Attached to the PVTOL CoM (EC case)

Like for the RG case, the EG case is subject to the same negative result presented in Sec. V-B. Therefore, for the same motivations of the rigid-case (see Secs. V-B and V-C) let us consider again the model in which $\mathrm{P}_{\mathrm{C}_1}$ coincides with P_{M}, i.e., $\mathbf{d}_1 = \mathbf{0}_{2\times 1}$, but this time with elastic-joint instead of a rigid one (see Fig. 3). This case is referred to as Case EC in Table I. In particular we are interested in finding whether, similarly to the RC case, also in this case the output $\mathbf{y} = [\mathbf{p}_m^T \ \theta_{12}]^T$ is exactly linearizing (i.e., flat).

Let us then consider as generalized coordinates $\mathbf{q} = [\mathbf{p}_m^T \ \theta_1 \ \theta_{12} \ \theta_{1m}]^T \in \mathbb{R}^5$, where, we remind that $\mathbf{p}_m = \mathbf{p}_{c_1}$. In this case the inertia matrix is

$$\mathbf{M} = \begin{pmatrix} m_s \mathbf{I}_2 & * & * & * \\ \mathbf{0}_{1\times 2} & J_1 & * & * \\ \boldsymbol{\beta}^T(\theta_{12}) & 0 & m_B - J_m & * \\ \mathbf{0}_{1\times 2} & 0 & 0 & J_m \end{pmatrix} = \mathbf{M}^T \in \mathbb{R}^{5\times 5}, \tag{73}$$

the centrifugal/Coriolis and gravitational forces are

$$\mathbf{c}(\mathbf{q}, \dot{\mathbf{q}}) = \begin{bmatrix} \bar{\beta}_1(\theta_{12}) \dot{\theta}_{12}^2 \\ \bar{\beta}_2(\theta_{12}) \dot{\theta}_{12}^2 \\ 0 \\ 0 \\ 0 \end{bmatrix}, \quad \mathbf{g}(\mathbf{q}) = \begin{bmatrix} 0 \\ -m_s \bar{g} \\ 0 \\ g_4(\theta_{12}) \\ 0 \end{bmatrix}, \tag{74}$$

and notice that the elastic forces $\mathbf{f}_E$ are the same as in (50). Finally the control input matrix from generalized forces is

$$\mathbf{G}(\mathbf{q}) = \begin{pmatrix} -\sin(\theta_1) & 0 & 0 \\ -\cos(\theta_1) & 0 & 0 \\ d_{G_x} & 1 & -1 \\ 0 & 0 & 0 \\ 0 & 0 & 1 \end{pmatrix}. \tag{75}$$

Replacing $\mathbf{M}$, $\mathbf{c}$, $\mathbf{g}$, $\mathbf{G}$ and $\mathbf{f}_E$ in (1) we can derive the explicit dependency of each entry of $\ddot{\mathbf{q}}$, here summarized:[15]

$$\begin{aligned} \ddot{x}_m &= f_1(\theta_1, \theta_{12}, \dot{\theta}_{12}, \theta_{1m}, u_t) \\ \ddot{z}_m &= f_2(\theta_1, \theta_{12}, \dot{\theta}_{12}, \theta_{1m}, u_t) \\ \ddot{\theta}_1 &= f_3(u_t, u_r, \tau) \\ \ddot{\theta}_{12} &= f_4(\theta_1, \theta_{12}, \dot{\theta}_{12}, \theta_{1m}, u_t) \\ \ddot{\theta}_{1m} &= f_5(\theta_{1m}, \theta_{12}, \tau). \end{aligned} \tag{76}$$

Let us now consider the output $\mathbf{y} = [\mathbf{p}_m^T, \theta_{12}]^T \in \mathbb{R}^3$ and try to find s_1, s_2, and s_3 that satisfy Condition 1 of Definition 1.

If we compare Case RC with Case EC we have that in the former case $n = 8$ while $n = 10$ in the latter, which implies that a higher total relative degree has to be reached in Case EC to fulfill Condition 1. If we then compare (76) to (33) we see that the only input appearing in Case EC for $\ddot{\mathbf{y}}$ is u_t while in Case RC both u_t and τ appear. This is a good sign since in Case RC we had to choose both $s_1 = 2$ and $s_2 = 2$ thus raising $\bar{n}$ to $8 + 4 = 12$ while in Case EC we probably do not need to add two integrators on the τ channel because τ it is not appearing already in $\ddot{\mathbf{y}}$.

Let us consider then $s_1 = 2$, and $s_2 = s_3 = 0$. With this choice the new input is $\bar{\mathbf{u}} = [\dot{u}_t \ u_r \ \tau]^T \in \mathbb{R}^3$, new state $\bar{\mathbf{x}} = [\mathbf{q}^T \ \dot{\mathbf{q}}^T \ u_t \ \dot{u}_t]^T \in \mathbb{R}^{12}$, and $\bar{n} = 12$.

The functional dependency of the derivatives of $\mathbf{y}$ can be written as follows:

$$\ddot{\mathbf{y}} = \boldsymbol{\xi}_1(\theta_1, \theta_{12}, \dot{\theta}_{12}, \theta_{1m}, u_t). \tag{77}$$

Let us now further derivate the output until the input appears. Using $\ddot{\theta}_{12}$ from (76) we can write

$$\dddot{\mathbf{y}} = \boldsymbol{\xi}_2(\theta_1, \theta_{12}, \theta_{1m}, \dot{\theta}_1, \dot{\theta}_{12}, \dot{\theta}_{1m}, u_t, \dot{u}_t). \tag{78}$$

Using $\ddot{\theta}_1$ from (76) we can write

$$\ddddot{\mathbf{y}} = \boldsymbol{\xi}_3(\theta_1, \theta_{12}, \theta_{1m}, \dot{\theta}_1, \dot{\theta}_{12}, \dot{\theta}_{1m}, u_t, \dot{u}_t, \ddot{u}_t, u_r, \tau)$$

in which the new inputs appear linearly, therefore $r_1 = r_2 = r_3 = 4$ and thus $r = 12 = \bar{n}$, which means that the Condition 1 of Definition 1 is satisfied. Therefore it is now worth to analytically search for the invertibility domain of $\bar{\mathbf{G}}(\bar{\mathbf{x}})$, which is given in the next result.

Proposition 4. *The vectors $[\mathbf{p}_c^T \ \theta_{12}]^T$, $[\mathbf{p}_m^T \ \theta_{12}]^T$ and $[\mathbf{p}_e^T \ \theta_{12}]^T$ are all exactly linearizing output via dynamic feedback for the coinciding model with elastic-joint arm (Case EC), as long as $u_t \neq 0$ and $k_e \neq 0$ (if the elasticity is linear). As a consequence, they are also flat outputs.*

Proof. For $[\mathbf{p}_c^T \ \theta_{12}]^T$ this descends from Proposition 3 since Case EC is a special case of Case EG. Concerning $[\mathbf{p}_e^T \ \theta_{12}]^T$,

[14] Detailed analytical computations of these values are given in the technical attachment. http://homepages.laas.fr/afranchi/files/J/TR-Yuesksel-Franchi.zip open with password: T-Ro2016.

[15] Again, also in this case, if one develops the computations can see that $\ddot{\theta}_{12}$ does not depend on $\dot{\theta}_{12}$ since the terms depending on $\dot{\theta}_{12}$ cancel out each other.

it is enough to prove the flatness of $[\mathbf{p}_m^T\ \theta_{12}]^T$ and apply (24). In the following we then prove only the flatness of $[\mathbf{p}_m^T\ \theta_{12}]^T$.

First, notice that the inertia matrix cannot be decoupled as nicely as in Case EG. However, we can re-concatenate the generalized coordinates in the form of; $\tilde{\mathbf{q}} = \mathbf{S}\mathbf{q} = [\mathbf{p}_m^T\ \theta_{12}\ \theta_1\ \theta_{1m}]^T \in \mathbb{R}^5$, where $\mathbf{S}$ is an orthogonal selection matrix

$$\mathbf{S} = \begin{pmatrix} 1&0&0&0&0\\ 0&1&0&0&0\\ 0&0&0&1&0\\ 0&0&1&0&0\\ 0&0&0&0&1 \end{pmatrix} = \mathbf{S}^T \in \mathbb{R}^{5\times 5}. \tag{79}$$

The new inertia matrix becomes $\tilde{\mathbf{M}} = \mathbf{S}^T\mathbf{M}\mathbf{S}$, where

$$\tilde{\mathbf{M}} = \left(\begin{array}{c|c} \tilde{\mathbf{M}}_{11} & \mathbf{0}_{3\times 2} \\ \hline \mathbf{0}_{2\times 3} & \tilde{\mathbf{M}}_{22} \end{array}\right), \tilde{\mathbf{M}}_{11} = \left(\begin{array}{c|c} m_s\mathbf{I}_2 & \boldsymbol{\beta} \\ \hline \boldsymbol{\beta}^T & m_B - J_m \end{array}\right) \in \mathbb{R}^{3\times 3}$$
$$\tilde{\mathbf{M}}_{22} = \left(\begin{array}{c|c} J_1 & 0 \\ \hline 0 & J_m \end{array}\right) \in \mathbb{R}^{2\times 2}; \tag{80}$$

the Coriolis/centrifugal forces become $\tilde{\mathbf{c}} = \mathbf{S}\mathbf{c}$, where $\mathbf{c}$ is available from (74); the gravitational forces become $\tilde{\mathbf{g}} = \mathbf{S}\mathbf{g}$, where $\mathbf{g}$ is available from (74); the elastic forces become $\tilde{\mathbf{f}}_E = \mathbf{S}\mathbf{f}_E$, where $\mathbf{f}_E$ is available from (50); and the input matrix becomes $\tilde{\mathbf{G}} = \mathbf{S}\mathbf{G}$, where $\mathbf{G}$ is available from (75).

Then, we obtain

$$\ddot{\tilde{\mathbf{q}}} = \mathbf{W}\left(\begin{array}{c} \begin{pmatrix}\mathbf{v}u_t\\0\end{pmatrix} + \begin{pmatrix}\mathbf{0}_{2\times 1}\\ k_e(\theta_{1m}-\theta_{12})\end{pmatrix} - \begin{pmatrix}\bar{\boldsymbol{\beta}}\dot{\theta}_{12}^2\\0\end{pmatrix} + \begin{pmatrix}0\\ m_s\bar{g}\\ -g_4(\theta_{12})\end{pmatrix} \\ \hline \begin{pmatrix}d_{G_x}u_t + u_r - \tau\\ \tau\end{pmatrix} + \begin{pmatrix}0\\ k_e(\theta_{12}-\theta_{1m})\end{pmatrix} \end{array}\right), \tag{81}$$

where $\mathbf{v}$ is as in (61a). Notice that $\mathbf{W} = \tilde{\mathbf{M}}^{-1}$, where

$$\mathbf{W} = \left(\begin{array}{c|c} \mathbf{W}_{11} \in \mathbb{R}^{3\times 3} & \mathbf{0}_{3\times 2} \\ \hline \mathbf{0}_{2\times 3} & \mathbf{W}_{22} \in \mathbb{R}^{2\times 2} \end{array}\right)$$
$$\mathbf{W}_{11} = \left(\begin{array}{c|c} \mathbf{W}_{11^1} \in \mathbb{R}^{2\times 2} & \mathbf{W}_{11^{21}}^T \\ \hline \mathbf{W}_{11^{21}} \in \mathbb{R}^{1\times 2} & W_{11^2} \in \mathbb{R} \end{array}\right) \in \mathbb{R}^{3\times 3}, \tag{82}$$

and $\mathbf{W}_{22} = \mathrm{diag}\{W_{22^1}, W_{22^2}\} \in \mathbb{R}^{2\times 2}$. Now notice that $\ddot{\mathbf{p}}_m$ is available from the first two equations, $\ddot{\theta}_{12}$ from the third, $\ddot{\theta}_1$ from fourth, and $\ddot{\theta}_{1m}$ from the last equation of (81). By differentiating $\ddot{\mathbf{p}}_m$ twice w.r.t. time, and utilizing $\ddot{\theta}_1$ and $\ddot{\theta}_{1m}$ from (81) we obtain

$$\dddot{\mathbf{p}}_m = \mathbf{W}_{11^1}\mathbf{v}\ddot{u}_t + \mathbf{W}_{11^1}\bar{\mathbf{v}}W_{22^1}u_t u_r - \mathbf{W}_{11^1}\bar{\mathbf{v}}W_{22^1}u_t\tau + \\ + \mathbf{W}_{11^{21}}^T W_{22^2}k_e\tau + \mathbf{h}_1(\tilde{\mathbf{q}}_r, \dot{\tilde{\mathbf{q}}}_r, u_t, \dot{u}_t), \tag{83}$$

where $\bar{\mathbf{v}}$ is as in (13), and $\tilde{\mathbf{q}}_r = \mathbf{S}\mathbf{q}_r$, with $\mathbf{q}_r = [\theta_1\ \theta_{12}\ \theta_{1m}]^T \in \mathbb{R}^3$. Furthermore, by differentiating $\ddot{\theta}_{12}$ twice w.r.t. time, and utilizing $\ddot{\theta}_1$ and $\ddot{\theta}_{1m}$ from (81) we get

$$\ddddot{\theta}_{12} = \mathbf{W}_{11^{21}}\mathbf{v}\ddot{u}_t + \mathbf{W}_{11^{21}}\bar{\mathbf{v}}W_{22^1}u_t u_r - \mathbf{W}_{11^{21}}\bar{\mathbf{v}}W_{22^1}u_t\tau + \\ + W_{11^2}W_{22^2}k_e\tau + h_2(\tilde{\mathbf{q}}_r, \dot{\tilde{\mathbf{q}}}_r, u_t, \dot{u}_t). \tag{84}$$

Then using (83) and (84) we can write

$$\begin{pmatrix}\dddot{\mathbf{p}}_m\\ \ddddot{\theta}_{12}\end{pmatrix} = \mathbf{h}(\mathbf{q}_r, \dot{\mathbf{q}}_r, u_t, \dot{u}_t) + \bar{\mathbf{G}}\bar{\mathbf{u}}, \tag{85}$$

where $\mathbf{h} = [\mathbf{h}_1^T\ h_2]^T \in \mathbb{R}^{3\times 1}$ and

$$\bar{\mathbf{G}}\bar{\mathbf{u}} = \underbrace{\left(\begin{array}{c|c|c} \mathbf{W}_{11^1}\mathbf{v} & \mathbf{W}_{11^1}\bar{\mathbf{v}}W_{22^1}u_t & \bar{\mathbf{G}}_{13} \\ \hline \mathbf{W}_{11^{21}}\mathbf{v} & \mathbf{W}_{11^{21}}\bar{\mathbf{v}}W_{22^1}u_t & \bar{\mathbf{G}}_{23} \end{array}\right)}_{\bar{\mathbf{G}}\in\mathbb{R}^{3\times 3}} \underbrace{\begin{pmatrix}\ddot{u}_t\\ u_r\\ \tau\end{pmatrix}}_{\bar{\mathbf{u}}} \tag{86}$$

where

$$\bar{\mathbf{G}}_{13} = \mathbf{W}_{11^{21}}^T W_{22^2}k_e - \mathbf{W}_{11^1}\bar{\mathbf{v}}W_{22^1}u_t$$
$$\bar{\mathbf{G}}_{23} = W_{11^2}W_{22^2}k_e - \mathbf{W}_{11^{21}}\bar{\mathbf{v}}W_{22^1}u_t \tag{87}$$

and $\bar{\mathbf{G}}$ is the new input matrix, whose determinant is

$$|\bar{\mathbf{G}}| = -\frac{u_t k_e}{J_1 J_m m_s\left(J_2 m_s + m_2(m_1+m_m)\,\|\mathbf{d}_2\|_2^2\right)}, \tag{88}$$

which is always invertible as long as $u_t \neq 0$ and $k_e \neq 0$ (if the elasticity is linear). This proofs that $[\mathbf{p}_m^T\ \theta_{12}]^T$ is exact linearizing output for Case EC. From Fact 1 it is a flat output as well. □

Derivation of the Algebraic Map from the Flat Output

We shall show now the procedure to explicitly derive the algebraic map that relates $\ddot{\mathbf{p}}_m, \dddot{\mathbf{p}}_m, \ddddot{\mathbf{p}}_m, \theta_{12}, \dot{\theta}_{12}, \ddot{\theta}_{12}, \dddot{\theta}_{12}, \ddddot{\theta}_{12}$ with θ_1, $\dot{\theta}_1$, θ_{1m}, $\dot{\theta}_{1m}$, and $\mathbf{u}$.

Consider the position in $\mathscr{F}_W$ of the CoM of the overall system, as in (44). By substituting it in (21) and in (22), we find $u_t, \dot{u}_t, \ddot{u}_t$ and $\theta_1, \dot{\theta}_1, \ddot{\theta}_1$ as functions of $\mathbf{y}, \cdots, \ddddot{\mathbf{y}}$. Furthermore, from the fourth equation of the system dynamics we get

$$\theta_{1m} = \frac{\boldsymbol{\beta}^T\ddot{\mathbf{p}}_m + (m_B - J_m)\ddot{\theta}_{12} + g_4(\theta_{12}) + k_e\theta_{12}}{k_e}, \tag{89}$$

which is function of solely the flat outputs, i.e., $\theta_{1m} = \theta_{1m}(\mathbf{y}, \ddot{\mathbf{y}})$. Now, recalling that $g_4(\theta_{12}) = -\boldsymbol{\beta}(\theta_{12})\bar{g}\cdot\mathbf{e}_2$ with $\mathbf{e}_2 = [0\ 1]^T \in \mathbb{R}^2$, we can write

$$\dot{\theta}_{1m} = \frac{\boldsymbol{\beta}^T\dddot{\mathbf{p}}_m + (m_B - J_m)\dddot{\theta}_{12} + (\bar{\boldsymbol{\beta}}^T\ddot{\mathbf{p}}_m - \bar{\boldsymbol{\beta}}\bar{g}\cdot\mathbf{e}_2 + k_e)\dot{\theta}_{12}}{k_e}$$
$$\ddot{\theta}_{1m} = \frac{\boldsymbol{\beta}^T\ddddot{\mathbf{p}}_m + (m_B - J_m)\ddddot{\theta}_{12} + 2\bar{\boldsymbol{\beta}}^T\dddot{\mathbf{p}}_m\dot{\theta}_{12}}{k_e} + \\ + \frac{(\bar{\boldsymbol{\beta}}^T\ddot{\mathbf{p}}_m - \bar{\boldsymbol{\beta}}\bar{g}\cdot\mathbf{e}_2 + k_e)\ddot{\theta}_{12} + (\boldsymbol{\beta}\bar{g}\cdot\mathbf{e}_2 - \boldsymbol{\beta}^T\ddot{\mathbf{p}}_m)\dot{\theta}_{12}^2}{k_e}, \tag{90}$$

which means $\dot{\theta}_{1m} = \dot{\theta}_{1m}(\mathbf{y}, \dot{\mathbf{y}}, \ddot{\mathbf{y}}, \dddot{\mathbf{y}})$, and $\ddot{\theta}_{1m} = \ddot{\theta}_{1m}(\mathbf{y}, \dot{\mathbf{y}}, \ddot{\mathbf{y}}, \dddot{\mathbf{y}}, \ddddot{\mathbf{y}})$. Moreover, one can rewrite the motor torque using the fifth equation of the system dynamics, namely

$$\tau = \tau(\theta_{12}, \theta_{1m}, \ddot{\theta}_{1m}) = J_m\ddot{\theta}_{1m} + k_e\theta_{1m} - k_e\theta_{12}, \tag{91}$$

where substituting θ_{1m} from (89) and $\ddot{\theta}_{1m}$ from (90), it is $\tau = \tau(\mathbf{y}, \dot{\mathbf{y}}, \ddot{\mathbf{y}}, \dddot{\mathbf{y}}, \ddddot{\mathbf{y}})$.

Finally the PVTOL torque is computed from the third equation of the system dynamics using

$$u_r = u_r(\ddot{\theta}_1, u_t, \tau) = J_1\ddot{\theta}_1 + \tau - d_{G_x}u_t, \tag{92}$$

Modeling Cases	Linearizing (Flat) Outputs	Relative Degree	New States	New Input
Case RG: Rigid-Joint Attached to a Generic Point • $P_{C_1} \neq P_M \neq P_G$ • $\mathbf{q} = [\mathbf{p}_c^T\ \theta_1\ \theta_{12}]^T \in \mathbb{R}^4$	$\mathbf{y} = [\mathbf{p}_c^T\ \theta_{12}]^T \in \mathbb{R}^3$	$\bar{\mathbf{y}} = [\dddot{\mathbf{p}}_c^T\ \ddot{\theta}_{12}]^T$ $r = 10$	$\bar{\mathbf{x}} = [\mathbf{q}^T\ \dot{\mathbf{q}}^T\ u_t\ \dot{u}_t]^T \in \mathbb{R}^{10}$ $\bar{n} = 10$	$\bar{\mathbf{u}} = [\ddot{u}_t\ u_r\ \tau]^T \in \mathbb{R}^3$
Case RC: Rigid-Joint Attached to the PVTOL CoM • $P_{C_1} \equiv P_M \neq P_G \implies \mathbf{p}_{c_1} = \mathbf{p}_m$ • $\mathbf{q} = [\mathbf{p}_m^T\ \theta_1\ \theta_{12}]^T \in \mathbb{R}^4$	also $\mathbf{y} = [\mathbf{p}_m^T\ \theta_{12}]^T \in \mathbb{R}^3$ and $\mathbf{y} = [\mathbf{p}_e^T\ \theta_{12}]^T \in \mathbb{R}^3$	$\bar{\mathbf{y}} = [\dddot{\mathbf{p}}_m^T\ \ddddot{\theta}_{12}]^T$ $r = 12$	$\bar{\mathbf{x}} = [\mathbf{q}^T\ \dot{\mathbf{q}}^T\ u_t\ \dot{u}_t\ \tau\ \dot{\tau}]^T \in \mathbb{R}^{12}$ $\bar{n} = 12$	$\bar{\mathbf{u}} = [\ddot{u}_t\ u_r\ \ddot{\tau}]^T \in \mathbb{R}^3$
Case EG: Elastic-Joint Attached to a Generic Point • $P_{C_1} \neq P_M \neq P_G$ • $\mathbf{q} = [\mathbf{p}_c^T\ \theta_1\ \theta_{12}\ \theta_r\ \theta_{1m}]^T \in \mathbb{R}^6$	$\mathbf{y} = [\mathbf{p}_c^T\ \theta_{12}]^T \mathbb{R}^3$	$\bar{\mathbf{y}} = [\mathbf{p}_c^{(6)^T}\ \ddddot{\theta}_{12}]^T$ $r = 16$	$\bar{\mathbf{x}} = [\mathbf{q}^T\ \dot{\mathbf{q}}^T\ u_t\ \dot{u}_t\ \ddot{u}_t\ \dddot{u}_t]^T \in \mathbb{R}^{16}$ $\bar{n} = 16$	$\bar{\mathbf{u}} = [\dddot{u}_t\ u_n\ \tau]^T \in \mathbb{R}^3$
Case EC: Elastic-Joint Attached to the PVTOL CoM • $P_{C_1} \equiv P_M \neq P_G \implies \mathbf{p}_{c_1} = \mathbf{p}_m$ • $\mathbf{q} = [\mathbf{p}_m^T\ \theta_1\ \theta_{12}, \theta_{1m}]^T \in \mathbb{R}^5$	also $\mathbf{y} = [\mathbf{p}_m^T\ \theta_{12}]^T \in \mathbb{R}^3$ and $\mathbf{y} = [\mathbf{p}_e^T\ \theta_{12}]^T \in \mathbb{R}^3$	$\bar{\mathbf{y}} = [\dddot{\mathbf{p}}_m^T\ \ddddot{\theta}_{12}]^T$ $r = 12$	$\bar{\mathbf{x}} = [\mathbf{q}^T\ \dot{\mathbf{q}}^T\ u_t\ \dot{u}_t]^T \in \mathbb{R}^{12}$ $\bar{n} = 12$	$\bar{\mathbf{u}} = [\ddot{u}_t\ u_r\ \tau]^T \in \mathbb{R}^3$

TABLE II: A summarizing table of the structural controllability properties for different models of PVTOL aerial manipulators equipped with a rigid-joint or an elastic-joint arm. The first column summarizes the properties of the four different cases, which are deeply studied in this paper. The remaining columns present the corresponding facts discovered in this paper. In every case the total number of states matches with the relative degree, which implies that no destabilizing internal dynamics will arise when an exact feedback linearization controller is applied to the system. This also implies the flatness of the corresponding output. See also Fig.6 of the technical attachment[1] showing how we used these properties and the controllers presented in this paper.

where utilizing $\ddot{\theta}_1$ from (22) and u_t from (21) by also taking (44) into consideration, and τ from (91), we can show that $u_r = u_r(\mathbf{y}, \dot{\mathbf{y}}, \ddot{\mathbf{y}}, \dddot{\mathbf{y}}, \ddddot{\mathbf{y}})$.

In summary, we obtained $\mathbf{p}_m = \mathbf{p}_m(\mathbf{y})$, $\dot{\mathbf{p}}_m = \dot{\mathbf{p}}_m(\dot{\mathbf{y}})$, $\ddot{\mathbf{p}}_c = \ddot{\mathbf{p}}_m(\ddot{\mathbf{y}})$ and $\theta_{12} = \theta_{12}(\mathbf{y})$, $\dot{\theta}_{12} = \dot{\theta}_{12}(\dot{\mathbf{y}})$, $\ddot{\theta}_{12} = \ddot{\theta}_{12}(\ddot{\mathbf{y}})$ from the definition; $u_t = u_t(\mathbf{y}, \dot{\mathbf{y}}, \ddot{\mathbf{y}})$, $\dot{u}_t = \dot{u}_t(\mathbf{y}, \dot{\mathbf{y}}, \ddot{\mathbf{y}}, \dddot{\mathbf{y}})$, $\ddot{u}_t = \ddot{u}_t(\mathbf{y}, \dot{\mathbf{y}}, \ddot{\mathbf{y}}, \dddot{\mathbf{y}}, \ddddot{\mathbf{y}})$ from (21) and $\theta_1 = \theta_1(\mathbf{y}, \dot{\mathbf{y}}, \ddot{\mathbf{y}})$, $\dot{\theta}_1 = \dot{\theta}_1(\mathbf{y}, \dot{\mathbf{y}}, \ddot{\mathbf{y}}, \dddot{\mathbf{y}})$, $\ddot{\theta}_1 = \ddot{\theta}_1(\mathbf{y}, \dot{\mathbf{y}}, \ddot{\mathbf{y}}, \dddot{\mathbf{y}}, \ddddot{\mathbf{y}})$ from (22) where for both $\mathbf{p}_c$ is obtained from (44); $\theta_{1m} = \theta_{1m}(\mathbf{y}, \ddot{\mathbf{y}})$, $\dot{\theta}_{1m} = \dot{\theta}_{1m}(\mathbf{y}, \dot{\mathbf{y}}, \ddot{\mathbf{y}}, \dddot{\mathbf{y}})$, $\ddot{\theta}_{1m} = \ddot{\theta}_{1m}(\mathbf{y}, \dot{\mathbf{y}}, \ddot{\mathbf{y}}, \dddot{\mathbf{y}}, \ddddot{\mathbf{y}})$ from (89)-(90); and finally $\tau = \tau(\mathbf{y}, \dot{\mathbf{y}}, \ddot{\mathbf{y}}, \dddot{\mathbf{y}}, \ddddot{\mathbf{y}})$ from (91) and $u_r = u_r(\mathbf{y}, \dot{\mathbf{y}}, \ddot{\mathbf{y}}, \dddot{\mathbf{y}}, \ddddot{\mathbf{y}})$ from (92). Hence we showed how the states and the control inputs of the system can be written as functions of the flat outputs and a finite number of their derivatives.

Remark 2. *Notice that in Case RC, both u_t and τ needed to be delayed twice with a double integrator, while for Case EC this holds only for only u_t, in order to match the condition on the relative degree and total number of states ($r = \bar{n}$) . This happens because the spring in Case EC introduces a second order linear system and hence further delaying for τ is not needed.*

VII. Using Flatness to Plan Optimal Trajectories

In this section we formalize the optimal control problem for planning the optimal trajectories of aerial manipulators which take into account the saturations of the actuators and the bounds of the system state. In order to generate trajectories that satisfy the system dynamics, we show here how to use the differential flatness property of the system in the planning phase. Another advantage of using differential flatness is that one can generate an initial guess of the trajectory by smoothly interpolating the flat output from its initial to final value and analytically compute the all states and control inputs of the system accordingly. In this way, a *warm start* to the optimal solver can be given, which reduces the computation time of the optimal trajectory.

Dynamic feasibility of the optimal trajectories is ensured by the smoothness of the flat output have. To obtain trajectories that are smooth enough, we use the extension of the system dynamics given in (1). In this paper we focus on the tasks performed by the end-effector of the aerial manipulators. Hence, and because of the reasons explained in Sec. V-B, we will use the models described as Case RC and Case EC. After presenting the dynamic extensions for Cases RC and EC, we then use them in the formalization of the optimal control problem together with their exact tracking controllers as presented in Sections V-C and Sec.VI-B, respectively.

A. Using Differential Flatness for Dynamic Extension

In Sec. V-C and in Sec. VI-B we showed the differentially flat outputs of the systems described as Case RC and Case EC, respectively. Now, let us use this knowledge to extend the system dynamics for generating the smooth trajectories.

1) Dynamic Extension for Case RC: Consider the system model in Section V-C. The system dynamics is summarized in (33), which can be written in the following form

$$\ddot{\mathbf{q}} = \mathbf{f}(\mathbf{q}, \dot{\mathbf{q}}, \mathbf{u}) \in \mathbb{R}^{4\times 1}. \tag{93}$$

The flat outputs are $\mathbf{y} = [\mathbf{p}_m^T \theta_{12}]^T$ (see Proposition 2) and the implicit functional dependencies of their derivatives are shown in (35) and (V-C). Also considering Table II we know that $\bar{\mathbf{x}} = [\mathbf{q}^T\ \dot{\mathbf{q}}^T\ u_t\ \dot{u}_t\ \tau\ \dot{\tau}]^T \in \mathbb{R}^{12}$ and $\bar{\mathbf{u}} = [\ddot{u}_t\ u_r\ \ddot{\tau}]^T \in \mathbb{R}^3$. Hence, we can write

$$\dot{\bar{\mathbf{x}}} = \begin{pmatrix} \mathbf{0}_4 & \mathbf{I}_4 & \mathbf{0}_4 \\ \mathbf{0}_4 & \mathbf{0}_4 & \mathbf{0}_4 \\ \mathbf{0}_4 & \mathbf{0}_4 & \mathbf{S} \end{pmatrix} \bar{\mathbf{x}} + \begin{bmatrix} \mathbf{0}_{4\times 1} \\ \mathbf{f}(\mathbf{q}, \dot{\mathbf{q}}, \mathbf{u}) \\ \mathbf{s}(\ddot{u}_t, \ddot{\tau}) \end{bmatrix} = \bar{\mathbf{f}}(\bar{\mathbf{x}}, \bar{\mathbf{u}}), \tag{94}$$

where $\mathbf{f}$ is available from (93) and

$$\mathbf{S} = \begin{pmatrix} 0 & 1 & 0 & 0 \\ 0 & 0 & 0 & 0 \\ 0 & 0 & 0 & 1 \\ 0 & 0 & 0 & 0 \end{pmatrix} \in \mathbb{R}^{4\times 4}, \quad \mathbf{s} = \begin{bmatrix} 0 \\ \ddot{u}_t \\ 0 \\ \ddot{\tau} \end{bmatrix} \in \mathbb{R}^4.$$

Later, we will use the extended system dynamics given in (94) for the optimization problem.

2) Dynamic Extension for Case EC: Consider the system model in Section VI-B. The system dynamics is summarized in (76), which can be written in the following form

$$\ddot{\mathbf{q}} = \mathbf{f}(\mathbf{q}, \dot{\mathbf{q}}, \mathbf{u}) \in \mathbb{R}^{5\times 1}. \tag{95}$$

The flat outputs are $\mathbf{y} = [\mathbf{p}_m^T \theta_{12}]^T$ (see Proposition 4) and the implicit functional dependencies of their derivatives are shown in (78) and (VI-B). Also considering Table II we know that $\bar{\mathbf{x}} = [\mathbf{q}^T \ \dot{\mathbf{q}}^T \ u_t \ \dot{u}_t]^T \in \mathbb{R}^{12}$ and $\bar{\mathbf{u}} = [\ddot{u}_t \ u_r \ \tau]^T \in \mathbb{R}^3$. Hence, we can write

$$\dot{\bar{\mathbf{x}}} = \begin{pmatrix} \mathbf{0}_5 & \mathbf{I}_5 & \mathbf{0}_{5\times 2} \\ \mathbf{0}_5 & \mathbf{0}_5 & \mathbf{0}_{5\times 2} \\ \mathbf{0}_{2\times 5} & \mathbf{0}_{2\times 5} & \mathbf{S} \end{pmatrix} \bar{\mathbf{x}} + \begin{bmatrix} \mathbf{0}_{5\times 1} \\ \mathbf{f}(\mathbf{q}, \dot{\mathbf{q}}, \mathbf{u}) \\ \mathbf{s}(\ddot{u}_t) \end{bmatrix} = \bar{\mathbf{f}}(\bar{\mathbf{x}}, \bar{\mathbf{u}}), \tag{96}$$

where $\mathbf{f}$ is available from (95) and

$$\mathbf{S} = \left(\begin{smallmatrix} 0 & 1 \\ 0 & 0 \end{smallmatrix}\right) \in \mathbb{R}^{2\times 2}, \quad \mathbf{s} = \left[\begin{smallmatrix} 0 \\ \ddot{u}_t \end{smallmatrix}\right] \in \mathbb{R}^2.$$

In the following, we will use the extended system dynamics given in (96) for the optimization problem.

B. Optimal Control Problem

We consider the following optimization problem

$$\begin{aligned} \underset{\bar{\mathbf{x}}(t), \bar{\mathbf{u}}(t)}{\text{minimize}} \quad & J(\bar{\mathbf{x}}(t), \bar{\mathbf{u}}(t), t_L) \\ \text{subject to,} \quad & \forall t \in [t_0, t_L] \\ & \dot{\bar{\mathbf{x}}} = \bar{\mathbf{f}}(\bar{\mathbf{x}}(t), \bar{\mathbf{u}}(t)), \bar{\mathbf{x}}(t_0) = \bar{\mathbf{x}}_0 \\ & \mathbf{q}_m \le \mathbf{q} \le \mathbf{q}_M, \quad \mathbf{u}_m \le \mathbf{u} \le \mathbf{u}_M \\ & \psi_m \le \psi \le \psi_M \end{aligned} \tag{97}$$

where $J : \bar{\mathbf{x}}, \bar{\mathbf{u}} \to \mathbb{R}$ is the cost function[16]; $\bar{\mathbf{f}}$ is the system dynamics available from (94) for Case RC, and from (96) for Case EC; $\mathbf{q}$ and $\mathbf{u}$ are the system coordinates and the inputs[17]; and $\bar{\mathbf{x}}_0$ are the initial conditions. Notice that ψ is the deflection of the elastic element, i.e. $\psi = \theta_e = \theta_2 - \theta_m$, and this condition is added only for Case EC.

Now we have a formal definition of an optimal control problem, which can be used to generate a trajectory for aerial manipulators described as Case RC and RE.

The dimension and hence the complexity of the system at hand is too high to solve it as an optimal control problem in an analytical way. A way to approaching the optimal control problem is to reduce the system complexity, as it is don, e.g., in [23], where authors used the angular velocity of the system as inputs, instead of force/torque inputs. This approach is not viable for aerial manipulators where the dynamical effects cannot be neglected. Therefore, in this paper we consider the full system dynamics and solve the optimization problem using the direct optimization method, such as the one presented in [34].

[16]For example, in Sec. VIII-D we consider the *aerial throwing task* in which the cost function is the throwing distance.

[17]Notice that both $\mathbf{q}$ and $\mathbf{u}$ are the part of $\bar{\mathbf{x}}$ in both Case RC and EC. Here by limiting the states and the control inputs of the robots, we also limit $\bar{\mathbf{x}}$.

Quantity	Symb.	Nom. Value/Range	Unit
PVTOL mass	m_1	1.00	kg
motor mass	m_m	0.20	kg
link mass	m_2	0.30	kg
rotating motor mass	m_r	0.05	kg
object mass	m_o	0.5	kg
PVTOL inertia	J_1	0.028	kgm^2
motor solid inertia	J_{ms}	0.0562e-06	kgm^2
motor inertia	J_m	0.4101	kgm^2
link inertia	J_2	0.004	kgm^2
dis. vec. betw. P_{C_1} & P_M	$\mathbf{d}_1$	$-[8\ 8]^T \leftrightarrow [8\ 8]^T$	cm
dis. vec. betw. P_{C_2} & P_M	$\mathbf{d}_2$	$[0\ 0.2]^T$	m
dis. vec. betw. P_{C_2} & P_E	$\mathbf{d}_e$	$[0\ 0.2]^T$	m
dis. vec. betw. P_{C_1} & P_G	$\mathbf{d}_G$	$[0.01\ 0.05]^T$	m
motor shaft radius	r_r	0.015	m
linear spring stiffness	k_e	$3 \leftrightarrow 30$	Nm/rad
motor gear ratio	g_r	270:1	-
PVTOL thrust range	T_t	$0.1 \leftrightarrow 28$	N
PVTOL torque range	T_r	$-3 \leftrightarrow 3$	Nm
Motor torque range	T_m	$-5 \leftrightarrow 5$	Nm
grasping time	t_g	2.67	s
impact duration	T_i	0.01	s

TABLE III: Nominal parameters of the simulated systems.

Non-idealities	Notation	Value	Unit
deviation in masses	δ_m	2	%
deviation in inertias	δ_i	10	%
deviation in $\mathbf{d}_2$	δ_2	$[0\ 0.01]^T$	m
deviation in $\mathbf{d}_G$	δ_G	$[0\ 0.01]^T$	m
deviation in spring constant k_e	δ_s	0,5,10	%
3-sigma Gauss. noise in pos.	$3\sigma_p$	0.01	m
3-sigma Gauss. noise in vel.	$3\sigma_v$	0.02	m/s
3-sigma Gauss. noise in θ_1	$3\sigma_1$	0.01	rad
3-sigma Gauss. noise in $\dot{\theta}_1$	$3\sigma_{d1}$	0.02	rad/s
3-sigma Gauss. noise in $\theta_2, \theta_m, \theta_e$	$3\sigma_2$	0.001	rad
3-sigma Gauss. noise in $\theta_2, \theta_m, \theta_e$	$3\sigma_{d2}$	0.002	rad/s

TABLE IV: Deviations from the nominal parameters and standard deviations of the noise used in the simulations. The controllers are not aware of the deviations and use instead the nominal values of Table III.

VIII. Realistic Numerical Validation

In this section we show the results of extensive simulative tests aimed at validating, in non-ideal conditions, the performances of the feedback controllers and optimal trajectory generators presented in the previous sections. We focus in particular on the algorithms developed for cases RC (Sec. V-C) and EC (Sec. VI-B) because they permit to control the end-effector pose, which is the typical task in practical applications. We also test the robustness of those algorithms (shortly denoted as the *RC controller* and the *EC controller* in the following) when applied to the more general RG and EG cases.

The controller actions are computed using noisy measurements and nominal (i.e., wrong) values of the system parameters. The system dynamics is integrated using the real parameters values (i.e., nominal + deviations). A summary

Quantities	Notation	Value	Unit
min/max limits of x_m	$\mathbf{q}_m(1) \leftrightarrow \mathbf{q}_M(1)$	-0.5 $\leftrightarrow$ 0.5	m
min/max limits of z_m	$\mathbf{q}_m(2) \leftrightarrow \mathbf{q}_M(2)$	-0.5	m
min/max limits of θ_1	$\mathbf{q}_m(3) \leftrightarrow \mathbf{q}_M(3)$	-45$\leftrightarrow$ 45	deg
min/max limits of θ_{12}	$\mathbf{q}_m(4) \leftrightarrow \mathbf{q}_M(4)$	-45 $\leftrightarrow$ 45	deg
min/max limits of ψ	$\psi_m \leftrightarrow \psi_M$	-20$\leftrightarrow$20	deg
min. limit of u_t, u_r, τ	$\mathbf{u}_m$	$[0.1\ -1.75\ -1.5]^T$	N
max. limit of u_t, u_r, τ	$\mathbf{u}_M$	$[28\ 1.75\ 1.5]^T$	N
desired z_m	z_m^*	-1	m
initial values Case RC	$\bar{\mathbf{x}}_0(1) \leftrightarrow \bar{\mathbf{x}}_0(12)$	$[0\ -1\ \mathbf{0}_{1\times 6}\ -m_s\bar{g}\ \mathbf{0}_{1\times 3}]^T$	-
initial values Case EC	$\bar{\mathbf{x}}_0(1) \leftrightarrow \bar{\mathbf{x}}_0(12)$	$[0\ -1\ \mathbf{0}_{1\times 8}\ -m_s\bar{g}\ 0]^T$	-

TABLE V: Physical limits used in the aerial throwing tasks.

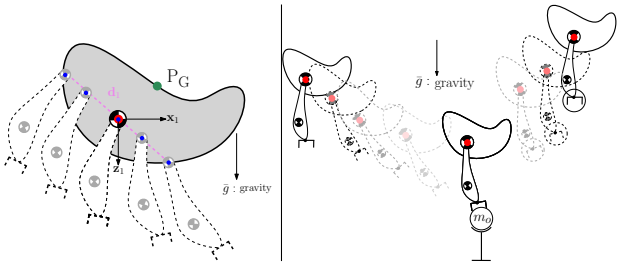


Fig. 4: – *Left:* the joint is not attached exactly at the PVTOL CoM: $\mathbf{d}_1$ spans the values given in Table III.
– *Right:* a sketch for grasping with PVTOL+arm system.

of the nominal values and the corresponding deviations, as well as of the noise characteristics, can be found in Tables III and IV. Nominal parameters, deviations, and noise are chosen very close to the values available on a real small-size aerial system equipped with standard sensors.

The system is simulated using an Ode8-solver at 1 kHz in Matlab Simulink. The noisy positions and velocity measurements are given to the controller at a rate of 30 Hz, similarly to what a commercial camera+IMU setup would provide. The rate of the noisy orientations and the angular velocities is 500 Hz, a realistic value for IMU attitude estimation and motor encoder readings.

In the dynamic models, the link attached to PVTOL is considered as a rod, whose inertia is computed using $J_2 = m_2 L^2/12$, where $L = ||\mathbf{d}_2 + \mathbf{d}_e||$. The motor inertia is computed as $J_m = g_r^2 J_{ms}$ where g_r is its gear reduction ratio, and $J_{ms} = m_r r_r^2/2$ is calculated by considering motor as a rotating solid cylinder. The stiffness range of the elastic actuator is chosen similar to the one from [35]. The physical limits of all the actuators are considered as hard thresholds and provided in Tables III and V.

In the next plots, for *nominal values* we mean the system behavior in the ideal case, i.e., as if the controllers were fully aware of the real parameters (nominal + deviation) of the system dynamics and there was neiter noise nor under-samplings in the measurements. The *actual values* represent instead the system behavior when the controllers use the nominal parameters, and under-sampled and noisy measurements.

A. Pole Placement Strategy

The feedback controllers used in the simulations have been explained in Sec. V-C and Sec. VI-B, in which we have analytically proven that the flat outputs are (in both cases) $\mathbf{y} = [\mathbf{p}_m \ \theta_{12}]^T$ (or, equivalently, $[\mathbf{p}_e \ \theta_{12}]^T$). Thanks to that results we can apply a nonlinear control loop to bring the system in the form (5). Then, given any 3-ple of desired trajectories of class C^3, $x_m^d(t)$, $z_m^d(t)$, $\theta_{12}^d(t)$ for x_m, z_m, and θ_{12}, respectively, the following outer control loop is used

$$\begin{aligned} v_{x_m} &= x_m^{d\,(4)} + K_{x1}e_x + K_{x2}e_x^{(1)} + K_{x3}e_x^{(2)} + K_{x4}e_x^{(3)} \\ v_{z_m} &= z_m^{d\,(4)} + K_{z1}e_z + K_{z2}e_z^{(1)} + K_{z3}e_z^{(2)} + K_{z4}e_z^{(3)} \\ v_{\theta_{12}} &= \theta_{12}^{d\,(4)} + K_{\theta 1}e_\theta + K_{\theta 2}e_\theta^{(1)} + K_{\theta 3}e_\theta^{(2)} + K_{\theta 4}e_\theta^{(3)} \end{aligned} \tag{98}$$

where $e_x = x_m^d - x_m$, $e_z = z_m^d - z_m$, $e_\theta = \theta_{12}^d - \theta_{12}$, and $K_{xi}, K_{zi}, K_{\theta i} \in \mathbb{R}_{>0}$, with $i = 1 \ldots 4$, are properly chosen gains.

We know that this control law will exponentially steer the three outputs along the desired trajectory, because we have analytically proven that the decoupling matrix $\bar{\mathbf{G}}$ is invertible almost everywhere. To compensate the errors due to uncertainties, an integral term $K_{i*}\int_{t0}^{tf} e_* dt$ is added in the outer loop of each channel, where $* := \{x, z, \theta\}$ and $K_{i*} \in \mathbb{R}_{>0}$.

Remark 3. *Notice that, as in any dynamic feedback linearization control, the obtained control law is a function of* only the measured state. *In fact, the derivatives of the output are algebraic function of the state thanks to the system model. Furthermore, the derivative of the actual inputs are internal variables of the state extension. Therefore there is no need to perform any numerical derivation to implement such controller but only to measure the state of the original system, i.e.,* $(\mathbf{q}, \dot{\mathbf{q}})$.

B. Test 1: Tracking a given Trajectory

The first set of tests validates the capabilities of the proposed controller of tracking a composite trajectory for the desired flat outputs x_m^d, z_m^d and θ_{12}^d in the non-ideal conditions. The plots of the results are shown in Fig. 5 In addition to the non-ideal conditions mentioned above, we tested the two controllers in the case that the arm joint is not perfectly attached to the PVTOL CoM, i.e., $\|\mathbf{d}_1\|$ is not exactly zero (see Fig. 4-Left). When doing so, an unstable behavior might appear if $\|\mathbf{d}_1\|$ is too large. However as long as $\|\mathbf{d}_1\|$ is kept in a reasonable bound the behavior remains stable, as illustrated in [36].

The main considerations are that: 1) the controllers do not need a perfect knowledge of the model parameters since the performances degrade smoothly and nicely with the increase of the parameter uncertainty; 2) the controllers work well with the typical noise, sampling and quantization that are presents in real systems; 3) the control effort in the case of the elastic-joint arm is larger with respect to the rigid-joint case. This happens because the controller needs suppress the tendency of the spring to oscillate at its natural frequency when steering the system along the desired trajectory

C. Test 2: Grasping an Object while Flying

In this section we first describe the scenario of grasping a stationary object using both the PVTOL+rigid-joint arm and the PVTOL+elastic-joint arm. A sketch depicting such task is given in the right side of Fig 4. The grasped object mass is $m_o > 0$. At time t_g (grasping time instant) the dynamic model of the simulated robot is updated accordingly to the grasping action and a disturbing impact force is also simulated based on the difference between the end-effector and the stationary mass velocities. More detail on the modeling of the aerial grasping can be found in the technical attachment of this paper[18].

1) Grasping with Rigid-joint Arm: Consider the model and the controller presented in Section V-C, i.e., Case RC. The composite trajectory used in the previous simulations is suitable for an aerial grasping task, at which an object with $m_o = 0.5$kg is to be grasped by the end-effector at time instant

[18] http://homepages.laas.fr/afranchi/files/J/TR-Yuesksel-Franchi.zip open with password: T-Ro2016.

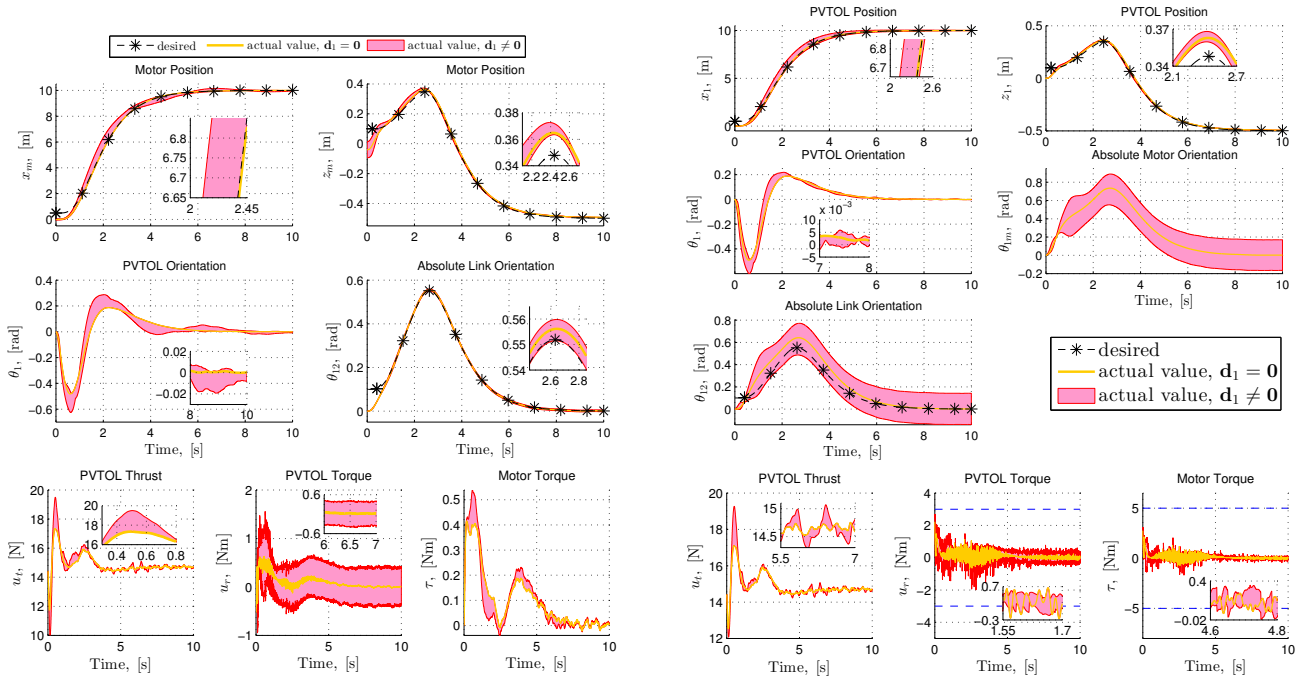


Fig. 5: Tracking of a given trajectory in presence of several non-ideal conditions: noise, parameter uncertainty, under-sampling, and attachement point of the joint different from the CoM (see Tables III and IV). – *Left:* rigid-joint case; – *Right:* elastic joint case. Several simulations are run: the maximum and minimum values among the different simulations are plotted with red solid curves, and pink-filled in between.

$t_g = 2.67$s. At this second, the joint arm is at its maximum orientation from the initial condition, at a high velocity in $+x$ direction, and at the beginning of its raising up again along the $-z$ axis ($+z$ is facing down because of the NED frame). Results are given in Fig. 6. Two cases are compared: known vs unknown grasped mass. After t_g, deviations from the desired trajectories are clearly seen for both cases. If the grasped mass is unknown, such deviation is higher for all the flat outputs. In the nominal case, the controller is fully aware of the end-effector velocity and mass, hence it generates high peaks in torques to counterbalance the impact. For the actual cases, controller is aware of the model with some deviations, hence it produces less reaction to the impacts compared to the nominal case, which results as worse tracking performance. However for the overall trajectory tracking problem, in the nominal case the controller tracks perfectly with less effort compared to the actual case, as also reported in Section VIII-B and in the technical attachment of this paper[18].

2) Grasping with Elastic-joint Arm: Consider the model presented in Section VI-B, i.e., Case EC. The same desired trajectory is used as in Section VIII-C1, where an object with $m_o = 0.5$kg has to be grasped by the end-effector at time instant $t_g = 2.67$s. Two cases are compared: grasping with low stiffness spring, $k_e = 8$ Nm and with high stiffness spring, $k_e = 30$ Nm. The results are given in Fig. 7. For both the low and the high stiffness cases, the tracking performance of the flat outputs are very close to each other. Moreover it is very similar to the results given in Fig. 6, with a clear difference in the absolute link orientation θ_{12}. However, the control effort is much more for Case EC than for Case RC. Using high stiffness joint mitigates this effect and results beneficial for the aerial grasping task. Finally, one can conclude this simulation set saying that for aerial grasping task and for tracking a generic trajectory Case RC is more advantageous than Case EC in terms of control effort.

D. Test 3: Throwing an Object while Flying

In this section we consider the *aerial throwing* task, in which an object is thrown from the end-effector of the aerial manipulator while the robot is flying. Such task is sketched in Fig. 8. Notice that aerial throwing problem is quite different from ground base robots throwing (see [18]), because in this case, the base of the robot is flying and it needs to compensate the dynamical effects while performing such task. A real scenario of aerial throwing task can be imagined as a situation, where the aerial manipulator is assigned to deliver a package, e.g. a first aid kit, in an hazardous environment, where the arrival point of the package is not suitable for the robot.

We define the following cost function

$$J = -J_d + \int_{t_0}^{t_L} (J_z + J_\tau) dT \quad \text{where}$$
$$J_d = d^2, \quad J_z = (z_m - z_m^*)^2, \quad J_\tau = \tau^2 \tag{99}$$

with upper-script $(^*)$ stands for the desired value and d is the thrown distance of the object, computed using the ballistic equation of the flying object, similar to [18]

$$d(\mathbf{y}, \dot{\mathbf{y}}) = x_e(\mathbf{y}) + \underbrace{\dot{x}_e(\mathbf{y}, \dot{\mathbf{y}}) t_f(\mathbf{y}, \dot{\mathbf{y}})}_{d_f}$$
$$t_f(\mathbf{y}, \dot{\mathbf{y}}) = \frac{1}{\bar{g}} \left(\dot{z}_e + \sqrt{\dot{z}_e^2 + 2\bar{g}(z_g - z_e)} \right) \tag{100}$$

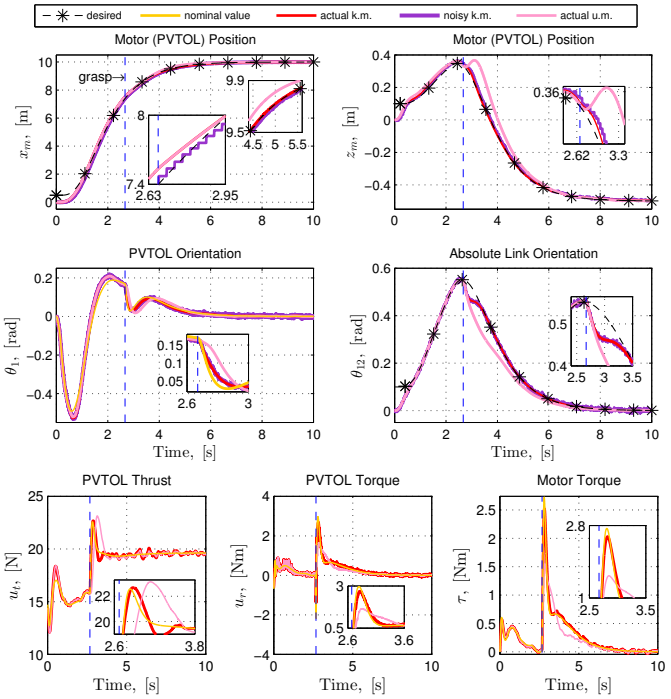


Fig. 6: Aerial grasping with a PVTOL+rigid-joint arm. The grasping instant is shown with a vertical blue dashed line. The nominal values are given with yellow solid curves. In the case of known grasped mass the actual values and noisy measurements are presented with red and purple solid curves, respectively. The pink solid curve shows the values in the case that the grasped mass is unknown.

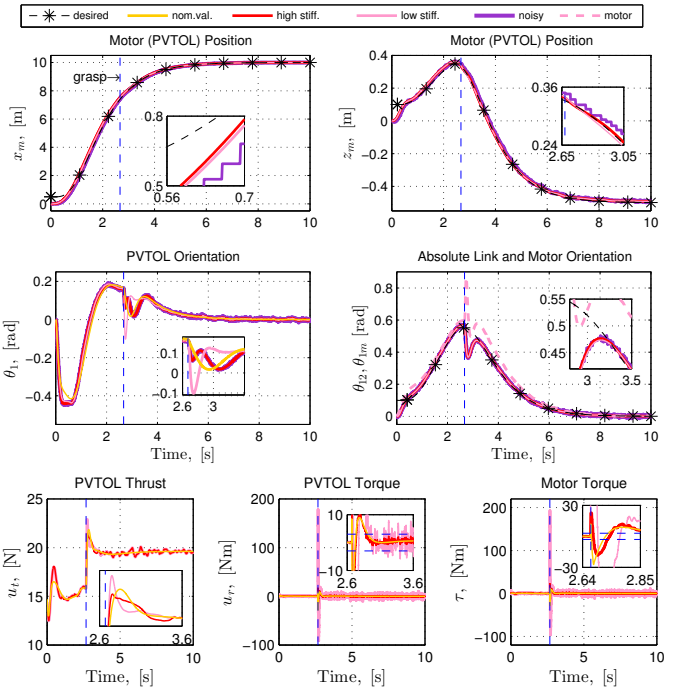


Fig. 7: Aerial grasping with a PVTOL+elastic-joint arm. The grasping instant is shown with a vertical blue dashed line. The nominal values are given with yellow solid curves. In the case in which a high stiffness elastic element is used, the actual values and noisy measurements are presented with red and purple solid curves, respectively. The pink solid curve instead the actual values in the case in which a low stiffness elastic element is used. A pink dashed curve is used only for actual motor values in case of low stiffness in the second plot on the right column. The horizontal blue dashed lines stand for the physical limits of the motor and PVTOL torques.

where recall that $\mathbf{p}_e = [x_e \; z_e]^T$ is the end-effector position and $\dot{\mathbf{p}}_e = [\dot{x}_e \; \dot{z}_e]^T$ is its velocity, where both can be computed using (24)[19]. The height of the ground is z_g, which is the altitude at which the object hits the ground. The total flight time of the thrown object is t_f, and the distance taken by the object after leaving the aerial manipulator is depicted with d_f. The cost function also includes the term J_z for keeping the aerial robot around its hovering height, and J_τ for minimizing the actuation costs.

By substituting (99) in the optimization problem described in (97), we compute the desired trajectories for the aerial manipulators described as Case RC and Case EC, for achieving aerial throwing task while respecting the system input and state boundaries. For solving this optimization problem, we used ACADO numerical optimizer [34]. The parameters for the simulation and the optimization problem is given in Table V.

The results are given in Fig. 9. The optimal trajectories computed using [34] are clearly enabling the aerial manipulator to throw the object to a far distance, at exactly $t_L = 1$ second, while keeping the PVTOL at the desired altitude. The results for Case RC (left of Fig. 9) and Case EC (right of Fig. 9) show that in both cases, the aerial robots are accelerating first backwards and then forwards along the x-axis to reach high linear velocities (due to the limits on x_m, see Table V). However notice that in Case EC, the aerial manipulator uses the potential energy stored in the elastic-joint for amplifying the link velocity. At the end, the aerial manipulator in Case

[19]Notice that the throwing distance d is a sole function of the flat outputs

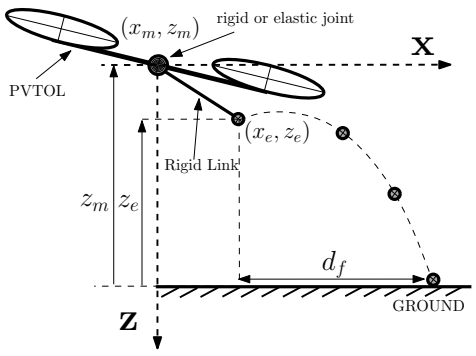


Fig. 8: Sketch of aerial throwing task using a PVTOL aerial manipulator. The ballistic trajectory of the thrown object is shown with dashed curve, and the distance taken by the object after leaving the aerial manipulator is shown with d_f.

EC achieves a higher throwing distance than the one of Case RC, by performing an explosive movement. This result is in the line with the high-speed swinging tests via link velocity amplification, presented in the technical attachment of this paper[18].

We notice that due to the term J_z in (99), the aerial manipulator tries to keep itself in the hover condition, which ensures that the system performs a stable flight. However this also limits the system to achieve a better throwing performance.

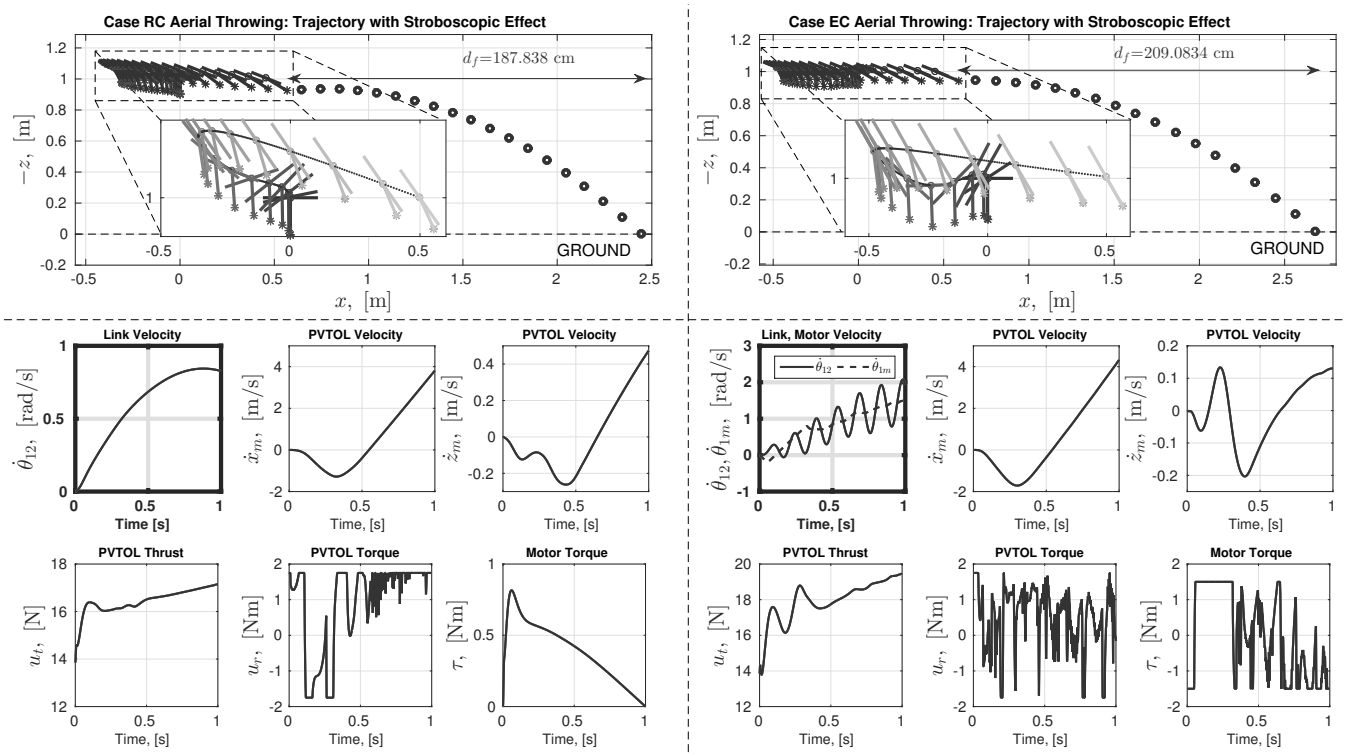


Fig. 9: Throwing object with the aerial manipulators in Case RC (left) and Case EC (right). Throwing is performed at $t_L = 1$ second.
– *Left:* Results for Case RC. The first plot on the top shows the trajectory of the aerial robot and the ballistic trajectory of the thrown object using stroboscopic effect. The trajectory of the aerial manipulator is separately emphasized in a zoomed subfigure. The thrown object hits the ground about 188 cm away from the end-effector. The link angular velocity, PVTOL linear velocities ($\dot{x}_m, \dot{z}_m$) and the control inputs are plotted below.
– *Right:* Results of Case EC. This time, the motor and the rigid link angular velocities are plotted together in the first figure of the second row, where dashed curve depicts the motor velocity and the solid one represents the rigid link velocity. Notice the link velocity amplification w.r.t. the motor velocity using the potential energy stored in the elastic-joint arm. The thrown object hits the ground at about 209 cm away from the end-effector.

Exploring different definitions of the cost function for aerial throwing is in the scope of our future studies.

	Trajectory Tracking	Aerial Grasping	Link Velocity Amplification	Aerial Throwing
Rigid Joint	+	+	-	-
Elastic Joint	-	-	+	+
Videos	v1.mp4, v2.mp4	v5.mp4	v3.mp4	v6.mp4

TABLE VI: Summary of the results showing which type of joint is more suitable for which simulations. The symbol '+' stands for 'more suitable', and '-' for 'less suitable'. The corresponding videos are cited as well, which are attached to this paper. Consider that another attached video named `v4.mp4` is showing the case when the joint has a *small* elasticity and friction. More details on is given in Section I-C of the technical attachment[18].

IX. Summary of the Simulations

The results presented in Section VIII and in the technical attachment of this paper[18] show that different choices for a PVTOL+joint arm design can be more or less suitable for different tasks. This is summarized in Table VI with the names of related files, provided as attachments to this paper.

X. Conclusions

In this paper we systematically presented and proved both the differential flatness property and the exact linearizing controllers for four different models of a PVTOL+joint arm mechanism: *i)* RG Case (Sec. V-A), *ii)* RC Case (Sec. V-C), *iii)* EG Case (Sec. VI-A), *iv)* EC Case (Sec. VI-B). Each of these cases outperforms another one for practical reasons as explained throughout the paper. We also presented formalization of an optimal control problem for aerial manipulators using their flatness property, and implemented it for the aerial throwing task. Using extensive and realistic simulation results we showed different tasks that are suitable for either rigid- or elastic-joint arm configuration. Namely, rigid-joint arm is more suitable for trajectory tracking or grasping tasks, while elastic-joint arm is more for the tasks requiring link velocity amplification such as aerial throwing. Furthermore we showed that the more generic models (Case RG and EG) can be controlled with the simpler controllers (RC Controller and EC Controller) for a bounded set of $\mathbf{d}_1 \neq 0$.

In the future we plan to apply presented controllers and use the differential flatness property of the PVTOL+joint arm systems on a real setup, developed based on our previous experiences [16]. Moreover, a clear trade-off between rigid- and elastic-joint arm setups directs us to use variable stiffness

actuators on board of an aerial vehicle, that can change their stiffness depending on which joint arm setup favors the task.

XI. Acknowledgements

During this work, Burak Yüksel has been co-funded by the Eiffel Excellence Scholarship Programme of the the French Ministry of Foreign Affairs and International Development, and by the Max Plank institute for Biological Cybernetics, Department of Human Perception, Cognition and Action, directed by Prof. Heinrich H. Bülthoff.

This work has been also partially funded by the European Union's Horizon 2020 research and innovation programme under grant agreement No 644271 AEROARMS

References

[1] V. Mistler, A. Benallegue, and N. K. M'Sirdi, "Exact linearization and noninteracting control of a 4 rotors helicopter via dynamic feedback," in *10th IEEE Int. Symp. on Robots and Human Interactive Communications*, Bordeaux, Paris, France, Sep. 2001, pp. 586–593.

[2] T. Lee, M. Leoky, and N. H. McClamroch, "Geometric tracking control of a quadrotor UAV on SE(3)," in *49th IEEE Conf. on Decision and Control*, Atlanta, GA, Dec. 2010, pp. 5420–5425.

[3] R. Mahony and V. Kumar, "Aerial robotics and the quadrotor," *IEEE Robotics & Automation Magazine*, vol. 19, no. 3, p. 19, 2012.

[4] A. Franchi, C. Secchi, M. Ryll, H. H. Bülthoff, and P. Robuffo Giordano, "Shared control: Balancing autonomy and human assistance with a group of quadrotor UAVs," *IEEE Robotics & Automation Magazine, Special Issue on Aerial Robotics and the Quadrotor Platform*, vol. 19, no. 3, pp. 57–68, 2012.

[5] B. Yüksel, C. Secchi, H. H. Bülthoff, and A. Franchi, "Reshaping the physical properties of a quadrotor through IDA-PBC and its application to aerial physical interaction," in *2014 IEEE Int. Conf. on Robotics and Automation*, Hong Kong, China, May. 2014, pp. 6258–6265.

[6] S. Kim, S. Choi, and H. J. Kim, "Aerial manipulation using a quadrotor with a two dof robotic arm," in *2013 IEEE/RSJ Int. Conf. on Intelligent Robots and Systems*, Tokyo, Japan, November 2013, pp. 4990–4995.

[7] M. Fumagalli, R. Naldi, A. Macchelli, R. Carloni, S. Stramigioli, and L. Marconi, "Modeling and control of a flying robot for contact inspection," in *2012 IEEE/RSJ Int. Conf. on Intelligent Robots and Systems*, Vilamoura, Portugal, Oct 2012, pp. 3532–3537.

[8] F. Forte, R. Naldi, A. Macchelli, and L. Marconi, "On the control of an aerial manipulator interacting with the environment," in *IEEE Int. Conf. on Robotics and Automation*, Hong Kong, China, June 2014, pp. 4487–4492.

[9] K. Kondak, K. Krieger, A. Albu-Schäffer, M. Schwarzbach, M. Laiacker, I. Maza, A. Rodriguez-Castano, and A. Ollero, "Closed-loop behavior of an autonomous helicopter equipped with a robotic arm for aerial manipulation tasks," *International Journal of Advanced Robotic Systems*, vol. 10, pp. 1–9, 2013.

[10] ARCAS, "EU Collab. Project ICT-287617," www.arcas-project.eu, 2011-2015.

[11] D. J. Lee and C. Ha, "Mechanics and control of quadrotors for tool operation," in *2012 ASME Dynamic Systems and Control Conference*, Fort Lauderdale, FL, Oct. 2012.

[12] V. Lippiello and F. Ruggiero, "Exploiting redundancy in cartesian impedance control of UAVs equipped with a robotic arm," in *2012 IEEE/RSJ Int. Conf. on Intelligent Robots and Systems*, Vilamoura, Portugal, Oct. 2012, pp. 3768–3773.

[13] H. Yang and D. Lee, "Dynamics and control of quadrotor with robotic manipulator," in *IEEE Int. Conf. on Robotics and Automation*, Hong Kong, China, June 2014, pp. 5544–5549.

[14] F. Ruggiero, M. A. Trujillo, R. Cano, H. Ascorbe, A. Viguria, C. Perez, V. Lippiello, A. Ollero, and B. Siciliano, "A multilayer control for multirotor uavs equipped with a servo robot arm," in *IEEE Int. Conf. on Robotics and Automation*, Seattle, Washington, May 2015, pp. 4014–4020.

[15] G. Heredia, A. E. J.-Cano, I. Sanchez, D. Llorente, V. Vega, J. Braga, J. A. Acosta, and A. Ollero, "Control of a multirotor outdoor aerial manipulator," in *IEEE/RSJ Int. Conf. on Intelligent Robots and Systems*, Chicago, IL, USA, September 2014, pp. 3417–3422.

[16] B. Yüksel, S. Mahboubi, C. Secchi, H. H. Bülthoff, and A. Franchi, "Design, identification and experimental testing of a light-weight flexible-joint arm for aerial physical interaction," in *2015 IEEE Int. Conf. on Robotics and Automation*, Seattle, WA, May 2015, pp. 870–876.

[17] SAPHARI, "EU Collab. Project FP7-ICT 287513," http://www.saphari.eu/, 2011-2015.

[18] D. J. Braun, F. Petit, and F. Huber, "Robots driven by compliant actuators: Optimal control under actuation constraints," *IEEE Trans. on Robotics*, vol. 29, no. 5, pp. 1085–1101, 2013.

[19] S. Haddadin and K. Krieger, "On impact decoupling properties of elastic robots and time optimal velocity maximization on joint level," in *2012 IEEE/RSJ Int. Conf. on Intelligent Robots and Systems*, Vilamoura, Portugal, October 2012, pp. 5089–5096.

[20] A. Suarez, G. Heredia, and A. Ollero, "Lightweight compliant arm for aerial manipulation," in *IEEE/RSJ Int. Conf. on Intelligent Robots and Systems*, Hamburg, Germany, September 2015, pp. 1627–1632.

[21] T. J. Koo and S. Sastry, "Differential flatness based fill authority helicopter control design," in *1999 IEEE Conf. on Decision and Control*, December 1999, pp. 1982–1987.

[22] A. De Luca, "Decoupling and feedback linearization of robots with mixed rigid/elastic joints," in *1996 IEEE Int. Conf. on Robotics and Automation*, Minneapolis, USA, Apr. 1996, pp. 816–821.

[23] S. Lupashin, A. Schöllig, M. Sherback, and R. D'Andrea, "A simple learning strategy for high-speed quadrocopter multi-flips," in *2010 IEEE Int. Conf. on Robotics and Automation*, Anchorage, AK, May 2010, pp. 1642–1648.

[24] S. Lupashin and R. D'Andrea, "Stabilization of a flying vehicle on a taut tether using inertial sensing," in *2013 IEEE/RSJ Int. Conf. on Intelligent Robots and Systems*, Tokyo, Japan, Nov 2013, pp. 2432–2438.

[25] J. Thomas, J. Polin, K. Sreenath, and V. Kumar, "Avian-Inspired Grasping for Quadrotor Micro UAVs," in *2013 ASME Int. Design Engineering Technical Conf. and Computers and Information in Engineering Conf.*, Portland, OR, Aug. 2013.

[26] R. Mahony, V. Kumar, and P. Corke, "Multirotor Aerial Vehicles: Modeling, Estimation, and Control of Quadrotor," *IEEE Robotics & Automation Magazine*, vol. 19, no. 3, pp. 20–32, 2012.

[27] A. Isidori, *Nonlinear Control Systems, 3rd edition*. Springer, 1995.

[28] K. Ogata, *Modern Control Engineering*, 5th ed. Prentice Hall, 2010.

[29] M. Fliess, J. Levine, and P. Rouchon, "Flatness and defect of nonlinear systems: Introductory theory and examples," *International Journal of Control*, vol. 61, pp. 1327–1361, 1995.

[30] R. M. Murray, M. Rathinam, and W. Sluis, "Differential flatness of mechanical control systems: A catalog of prototype systems," in *ASME Int. Mechanical Eng. Congress and Exposition*, San Francisco, CA, Nov. 1995.

[31] P. Martin, R. M. Murray, and P. Rouchon, "Flat systems, equivalence and trajectory generation," in *2003 CDS Technical Report*, 2003.

[32] A. De Luca and G. Oriolo, "Trajectory planning and control for planar robots with passive last joint," *The International Journal of Robotics Research*, vol. 21, no. 5-6, pp. 575–590, 2002.

[33] A. De Luca, "Decoupling and feedback linearization of robots with mixed rigid/elastic joints," *International Journal of Robust and Nonlinear Control*, vol. 8, no. 11, pp. 965–977, 1998. [Online]. Available: http://dx.doi.org/10.1002/(SICI)1099-1239(199809)8:11⟨965::AID-RNC371⟩3.0.CO;2-4

[34] B. Houska, H. Ferreau, and M. Diehl, "ACADO Toolkit – An Open Source Framework for Automatic Control and Dynamic Optimization," *Optimal Control Applications and Methods*, vol. 32, no. 3, pp. 298–312, 2011.

[35] QB-ROBOTICS, "Variable Stiffness Actuator," http://www.qbrobotics.com/.

[36] J. Hauser, S. Sastry, and G. Meyer, "Nonlinear control design for slightly non-minimum phase systems: Application to v/stol aircraft," *Automatica*, vol. 28, no. 4, pp. 665–679, 1992.